frontiers in Earth Science

ORIGINAL RESEARCH
published: 03 September 2021
doi: 10.3389/feart.2021.729955

Late Permian High-Ti Basalt in Western Guangxi, SW China and Its Link With the Emeishan Large Igneous Province: Geochronological and Geochemical Perspectives

Chenguang Zhang[1,2], *Renyu Zeng*[2,3,4]*, *Changming Li*[5,6], *Jian Jiang*[6], *Tianguo Wang*[2,3] and *Xingjun Shi*[1]

[1]School of Geographic Sciences, Xinyang Normal University, Xinyang, China, [2]Key Laboratory of Metallogenic Prediction of Nonferrous Metals and Geological Environment Monitoring (Central South University), Ministry of Education, Changsha, China, [3]State Key Laboratory of Nuclear Resources and Environment, East China University of Technology, Nanchang, China, [4]School of Earth Sciences, East China University of Technology, Nanchang, China, [5]China-ASEAN Geosciences Cooperation Center, Nanning, China, [6]Guangxi Institute of Geological Survey, Nanning, China

OPEN ACCESS

Edited by:
Kit Lai,
Universiti Brunei Darussalam, Brunei

Reviewed by:
Weimin Li,
Jilin University, China
Zhiqiang Feng,
Taiyuan University of Technology, China

***Correspondence:**
Renyu Zeng
zengrenyu@126.com

Specialty section:
This article was submitted to Volcanology, a section of the journal Frontiers in Earth Science

Received: 24 June 2021
Accepted: 19 August 2021
Published: 03 September 2021

Citation:
Zhang C, Zeng R, Li C, Jiang J, Wang T and Shi X (2021) Late Permian High-Ti Basalt in Western Guangxi, SW China and Its Link With the Emeishan Large Igneous Province: Geochronological and Geochemical Perspectives. Front. Earth Sci. 9:729955. doi: 10.3389/feart.2021.729955

High-Ti (Ti/Y) flood basalts are widely distributed in the Late Permian Emeishan large igneous province (LIP), SW China, and their spatial distribution and genetic mechanism are important to reveal the role of plume-lithosphere interactions in the LIP origin. Western Guangxi is located on the eastern edge of Emeishan LIP. To explore the genesis of the high-Ti basalt in western Guangxi and any genetic link with the Emeishan LIP, we performed whole-rock geochemical and Sr-Nd isotope and zircon U-Pb-Hf isotope analyses on the Longlin basalts from western Guangxi. The results indicate that the Longlin basalt from Tongdeng area has relatively high SiO_2 but low MgO and TFe_2O_3 contents. The rocks have zircon $\varepsilon Hf(t)$ = –0.42 to 6.41, whole-rock $(^{87}Sr/^{86}Sr)_i$ = 0.707167–0.707345, and $\varepsilon Nd(t)$ = –2.5 to –2.14. In contrast, the Longlin basalt from Zhoudong area has relatively low SiO_2 but high MgO and TFe_2O_3 contents. The rocks have whole-rock $(^{87}Sr/^{86}Sr)_i$ = 0.706181–0.706191 and $\varepsilon Nd(t)$ = –0.57 to 0.69. Four Longlin basalt samples display LREE enrichments and HREE depletions, and with indistinct δEu and δCe anomalies. LA-ICP-MS zircon U-Pb dating on three Longlin basalt samples (from different localities) yielded consistent weighted average age of 257.9 ± 2.6 Ma (MSWD = 0.55), 259.5 ± 0.75 Ma (MSWD = 3.0), and 256.7 ± 2.0 Ma (MSWD = 0.68), indicating a Late Permian emplacement. Considering the similar age and geochemical features between the Longlin basalt and Emeishan flood basalts, we interpret that the former is spatially, and temporally associated with the Emeishan LIP. Geochemical features show that the high-Ti basalts in western Guangxi resemble Deccan-type continental flood basalts (CFBs), which were derived by decompression melting of the mantle plume. Combined with previous geochemical studies, we suggest that the difference in Ti content and Ti/Y ratio in CFBs are related to the depth and melting degree of mantle source, in which high-Ti features may have been linked to low degree of partial melting in the deep mantle.

Keywords: Emeishan large igneous province, late Permian, Sr-Nd-Hf isotopes, basalt geochemistry, western Guangxi (SW China), Plume-lithosphere interaction

INTRODUCTION

Large igneous provinces (LIPs) are formed by voluminous mafic (and minor felsic) rocks emplaced in a short period of time, and are generally considered to be mantle plume-related but not directly related to normal ocean spreading and subduction (Coffin and Eldholm, 1994; Courtillot and Renne, 2003; Acocella, 2021), although recent works suggested that interaction between mantle plumes and subducting/subducted slabs may be plausible (Xu et al., 2019; Xu et al., 2021). LIPs are of great significance for studying of global environmental catastrophes and mass extinctions, mineral resources (esp. magmatic massive Cu-Ni-PGE sulfide and Fe-V-Ti oxide deposits), supercontinent reconstruction, and regional uplift (Wang and Zhou, 2005). Hence, petrogenesis of LIPs, such as the role of plume-lithosphere interaction in the origin of the continental flood basalts (CFB), and the origin of the high-Ti (Ti/Y), and low Ti mafic magmatism, has attracted much research attention (Fodor, 1987; Peate et al., 1999; Lai et al., 2012).

The Emeishan LIP is located in the western margin of the Yangtze craton and the eastern margin of the Tibetan plateau, SW China, and likely related to Late Permian mantle plume processes (Chung and Jahn, 1995; Li et al., 2008; Zhang, 2009). Complex tectonic events in the Sanjiang fold belt had strongly deformed the original distribution of the Emeishan LIP rock units (Xu et al., 2013). Besides, whether the basaltic rocks in the Song Hien

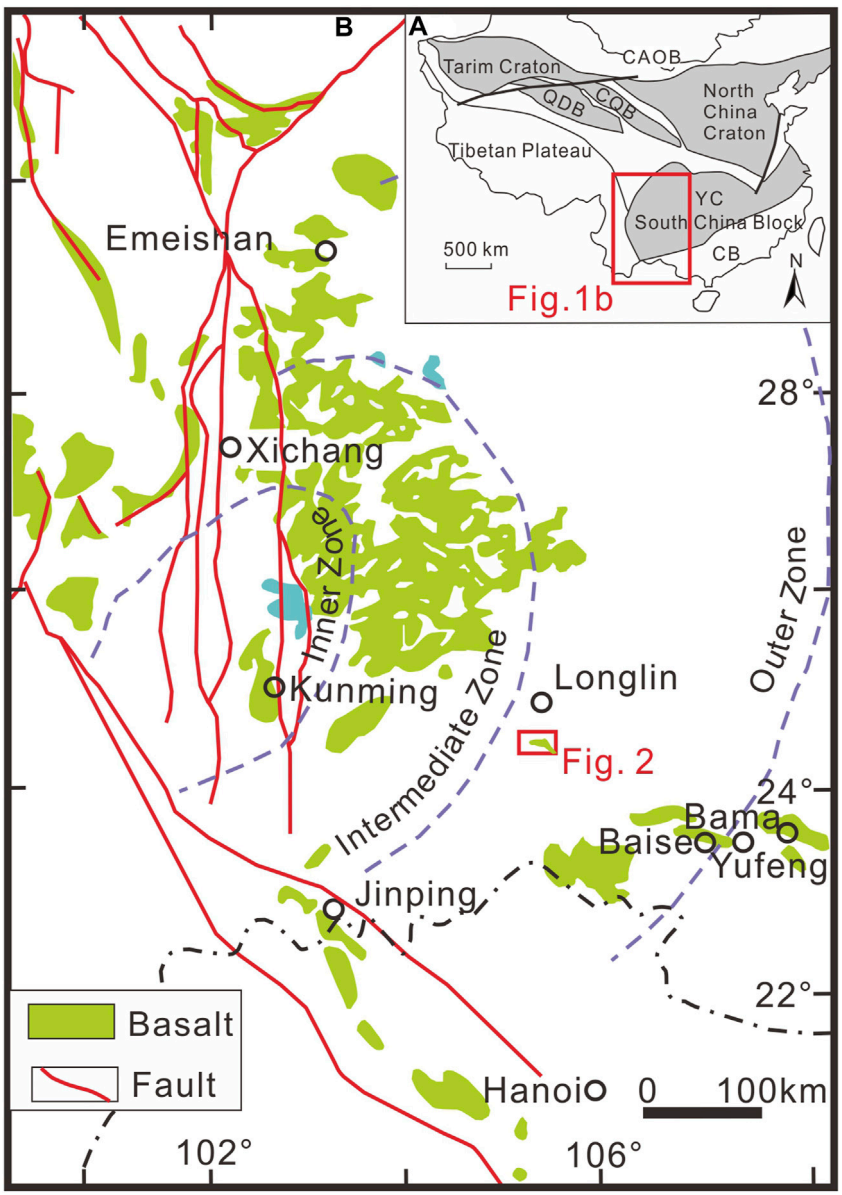

FIGURE 1 | Spatial distribution pattern of the Permian Emeishan flood basalts (outermost purple line denotes the possible extent of the outer zone, after Xu et al., 2001; He et al., 2003). YC–Yangtze Craton; CB–Cathaysia Block; CQB–Central Qilian Block; QDB–Qaidam Block; CAOB–Central Asian Orogenic Belt.

Tectonic Zone (NW Vietnam) are parts of the Emeishan LIP remains disputed (Halpin et al., 2016, and ref. therein). Therefore, it is of great significance to reveal the original spatial extent of CFB magmatism in the Emeishan LIP. Emeishan LIP consists mainly of flood basalts and associated mafic-ultramafic intrusions and (minor) felsic intrusions. The volcanics comprise mainly picrite, basalt and basaltic andesite, and can be divided into a high-Ti and low-Ti suite. This is similar to that in many other LIPs, such as the Siberian and Deccan Traps (Fodor, 1987; Peate et al., 1999; Fan et al., 2008). However, the validity of such Ti-based distinction is still disputed (Xu et al., 2001; Xu et al., 2004; Zhang et al., 2001; Shellnutt, 2014). Xu et al. (2001) considered that these high-Ti basalts were mantle plume-related, and formed by low-degree partial melting in the garnet stability field. However, Li et al. (2008) argued against substantial lithospheric mantle assimilation. Besides, some authors considered that the Emeishan basalts have a continuous TiO_2 range and should not be divided into two suites (Hou et al., 2011). For instance, Zhang (2009) considered that the high-Ti basalts may have formed by fractionation and accumulation of Fe-Ti oxides, whilst Hao et al. (2004) suggested that the high-Ti and low-Ti basalts are different fractionation products of the same parental magma.

Western Guangxi in SW China is located in the southwestern margin of the Yangtze craton (**Figure 1A**). It tectonically lies in the intersection between the Tethyan and Pacific tectonic domains. Mafic magmatism in the region is widespread and closely related to gold mineralization (Huang et al., 2015). Among the many mafic magmatic units, the Late Permian basalts are coeval with the Emeishan CFB, and generally display high-Ti (or high-Ti/Y) characteristics (Fan et al., 2008; Lai et al., 2012; Zhang and Xiao, 2014; Huang et al., 2015). However, petrogenetic setting of this magmatism is variably suggested to be 1) intra-oceanic setting related to the eastern Paleo-Tethys (Wu et al., 1993; Wu et al., 1997); 2) mantle plume related as part of the Emeishan (Liao et al., 2013; Zhang and Xiao, 2014; Huang et al., 2015). Besides, there are various views on the genesis of these rocks, including partial melting of the sub-continental lithospheric mantle (Lai et al., 2012), and mixing of plume-derived magma and continental lithosphere materials (Fan et al., 2008). In order to decipher the genesis and petrogenetic setting of these Late Permian basalts in western Guangxi, we conducted detailed field and petrographic observations on the high-Ti basalts in the Longlin area (western Guangxi), followed by zircon U-Pb-Hf isotope, as well as whole-rock elemental and Sr-Nd isotope analyses. Our findings constrain the formation timing and petrogenetic setting of the Longlin basalts, and explore the spatial distribution of Emeishan LIP and the genesis of high Ti-basaltic magmatism in western Guangxi.

GEOLOGICAL BACKGROUND AND PETROGRAPHIC FEATURES

The study area is located in the northern part of the Nanpanjiang-Youjiang rift basin in western Guangxi (**Figure 1**). Local tectonism is strong, and has undergone the Caledonian (Early Paleozoic), Variscan (Late Paleozoic), Indosinian (Triassic), Yanshanian (Jurassic-Cretaceous), and Himalayan (Cenozoic) tectonic cycles (Xu et al., 2013). The Caledonian orogeny may have closed the early Paleozoic South China ocean basin, forming the folded basement of the region. Afterward, the Indosinian orogeny terminated the pelagic sedimentation in South China, forming the complex tectonic framework of the region.

The study area is mainly covered by pelagic sedimentary rocks of Cambrian and Devonian to Triassic ages (**Figure 2**). The Cambrian rocks (total outcrop size: 60 km^2) comprise mainly carbonates, which are mainly distributed at Shechang and minor at Maxiong, Shuidong, Ganhao, and Poyan of the Xinzhou-Pingban counties (Li et al., 2019). Upper Paleozoic rocks (total outcrop size: 814 km^2) comprise mainly carbonates and minor clastics, of which the carbonate rocks are mainly distributed in the platforms and the limbs of the Shechang anticline, as well as in the northeastern part of the study area (Li et al., 2019). The clastic rocks are mainly distributed in the periphery of the platforms and in the southern limb of the Shechang anticline. Thick Triassic turbidite sequences are widely distributed in the deep-water basins between the carbonate platforms (total outcrop size: 1,005 km^2) (Li et al., 2019).

Magmatic rocks are uncommon in the study area, and consist mainly of mafic volcanic and (minor) plutonic rocks (total outcrop size: 30.75 km^2) in the central and southwestern parts of western Guangxi, e.g., at Nawei, Tongdeng, Boli, and Xiaoren. The basalts occur mainly as interlayers among the Middle Permian Sidazhai Formation and Upper Permian Linghao Formation (**Figure 3A**). Minor tuffaceous rocks were also found, and there is no discernible alteration in the wallrocks. Grain size decreases toward the intrusive margin, and vesicle and almond/pillow structure are uncommon. As shown in **Figure 4**, there are three layers of basalt in the Linghao Formation, with the thickness of 65, 15, and 10 m from bottom to top. The bottom of the first basalt layer consists of the Linghao Formation siltstone, and the top of each layer consists of volcaniclastic rocks. Eight least-altered samples (from Tongdeng, Xiaoren, and Zhoudong) were collected from the Linghao Formation basalt. The rocks are grey-greyish green and porphyritic (**Figure 3B**). Compositionally, the rocks contain mainly pyroxene (40–45%) and plagioclase (47–52%), together with minor biotite, ilmenite, pyrite, and pyrrhotite (**Figure 3C**). The basalts have phenocrysts of pyroxene and plagioclase (grain size: 0.5–1.2 mm). The pyroxene is subhedral-anhedral elongated and partly ilmenite-altered, whilst the plagioclase is elongated and partly epidote-altered. Fine-grained pyroxene, sphene, and serpentine occur as interstitial minerals (**Figure 3D**).

ANALYSIS METHODS

Major oxide concentrations were measured by wave-dispersive X-ray fluorescence (XRF) spectrometry at the

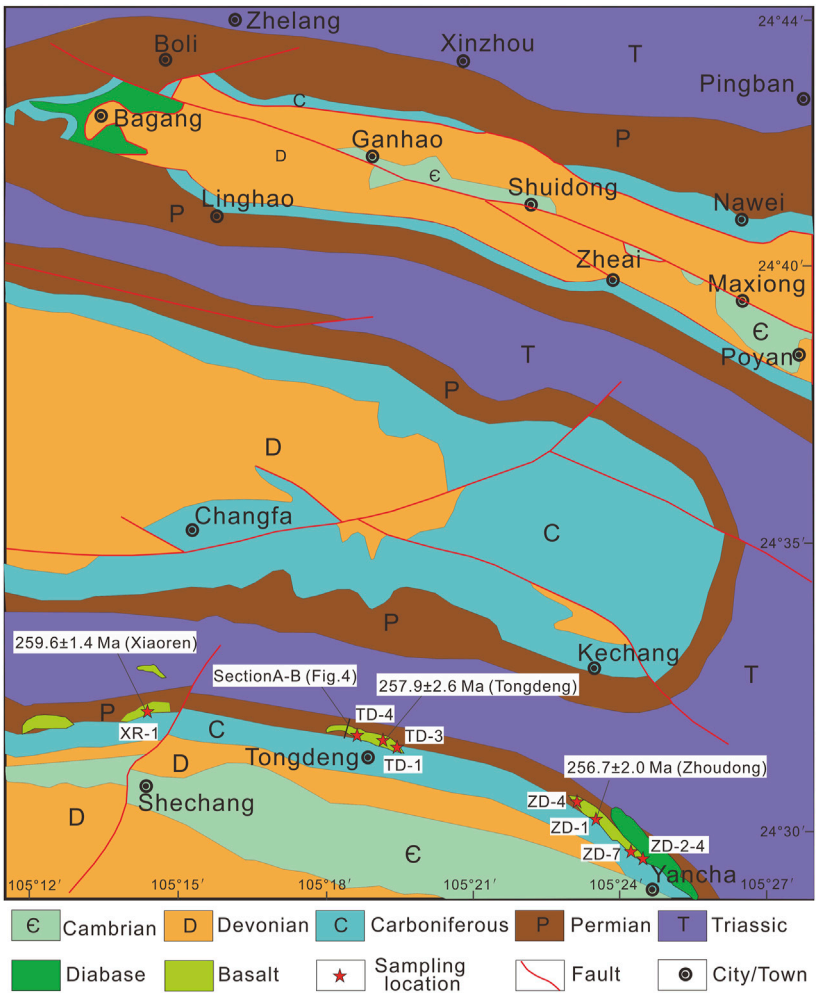

FIGURE 2 | Geologic sketch map of the Longlin area in western Guangxi.

Analytical Chemistry and Testing Services (ALS) Chemex Co. Ltd. (ALS Geochemistry method ME-XRF26). Fused glass disks with lithium borate were used and the analytical precisions were better than ± 0.01%, estimated from repeated analyses of the standards OREAS 146 and SY-4. Trace element concentrations of the samples were determined by a Perkin-Elmer ELAN 6000 inductively coupled plasma mass spectrometry (ICP-MS) after acid digestion in high-pressure Teflon bombs at the GIG-CAS (ALS Geochemistry method ME-MS81). The analytical errors were <5% for rare earth element (REE) and high field strength element (HFSE), and 5–10% for the other elements, based on repetitive analyses of standards NCSDC47009 and SARM-5. Detailed analytical procedures followed those outlined by Zhang et al. (2019).

Whole-rock Sr-Nd isotope analysis was conducted at the Isotope Geochemistry Laboratory, Wuhan Center of Geological Survey (China Geological Survey), using a Triton and MAT 261 thermal ionization mass spectrometer. The chemical analysis was monitored by the GBW04411, GBW04419 and NBS607 procedures, and the equipment conditions by the NBS987, NBS981 and JNDI procedures. Detailed analytical procedures were as described by Wang et al. (2015).

The CL images were performed using the TIMA analysis in the Chengpu Geological Testing Co. Ltd., Langfang, China. LA-ICP-MS zircon U-Pb dating was conducted at the Key Laboratory of Institute Continental Collision and Plateau Uplift, Tibetan Plateau Research (Chinese Academy of Sciences) analysis. The analysis used a UP193 F × 193 nm ArF ablation system coupled with an Agilent 7500a ICP-MS. Analytical conditions include 193 nm wavelength, < 4 ns pulse width, 35 μm spot size. 91,500 zircon was used as the external standard, and was analyzed between every six samples. The sample isotopic and elemental contents were calculated with the Glitter 4.5 software, whilst the Pb isotope calibration and U-Pb age calculation was performed with the ComPbcorr#3_18 (Andersen, 2002), and Isoplot 4.15 (Ludwig, 2003), respectively.

Zircon Lu-Hf isotope analysis was conducted at the State Key Laboratory of Geological Processes and Mineral

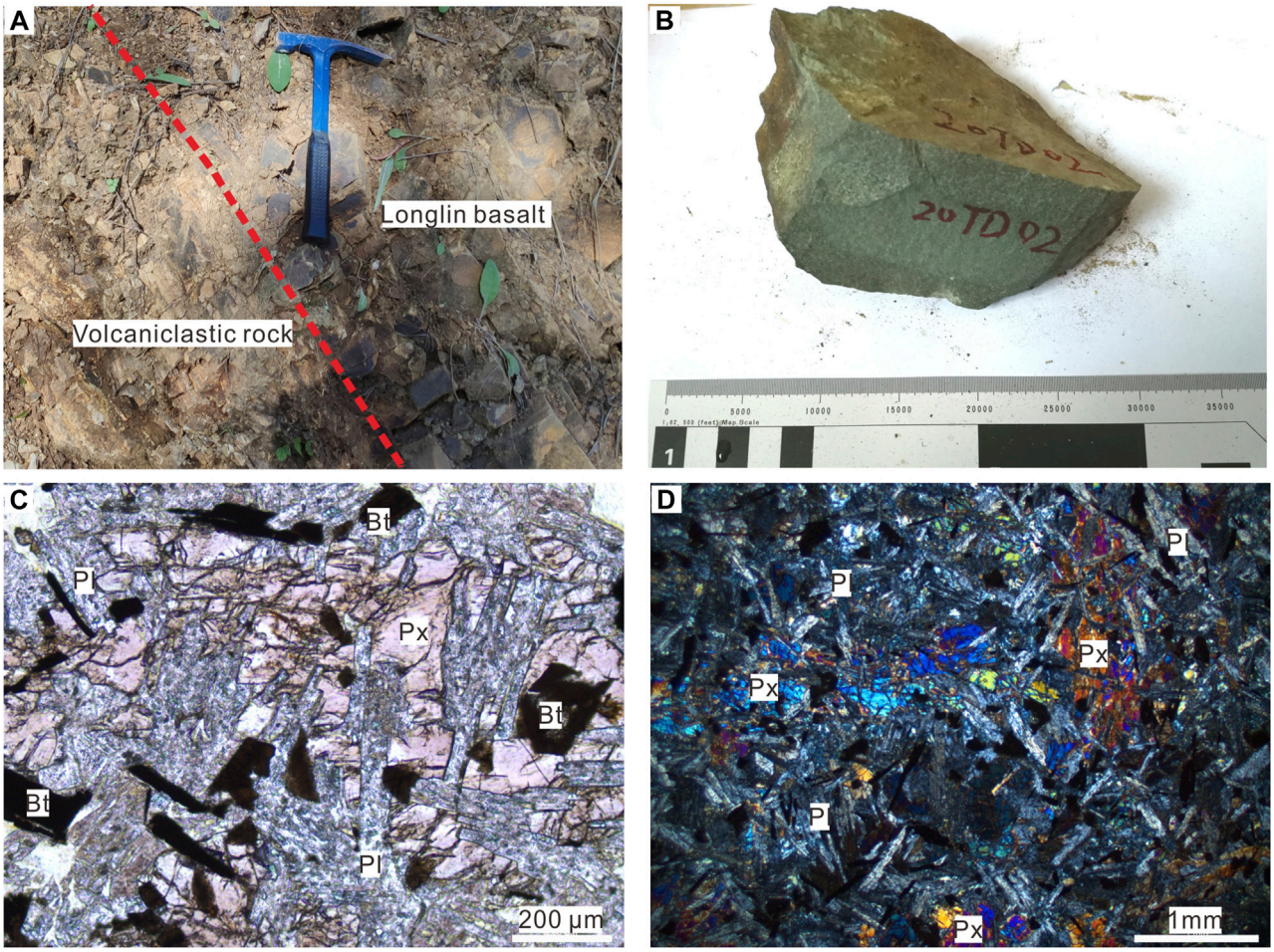

FIGURE 3 | Photos of **(A)** field outcrop, **(B)** hand-specimen, and **(C–D)** thin-section microscopy (c: PPL, d: XPL) of the Longlin basalts.

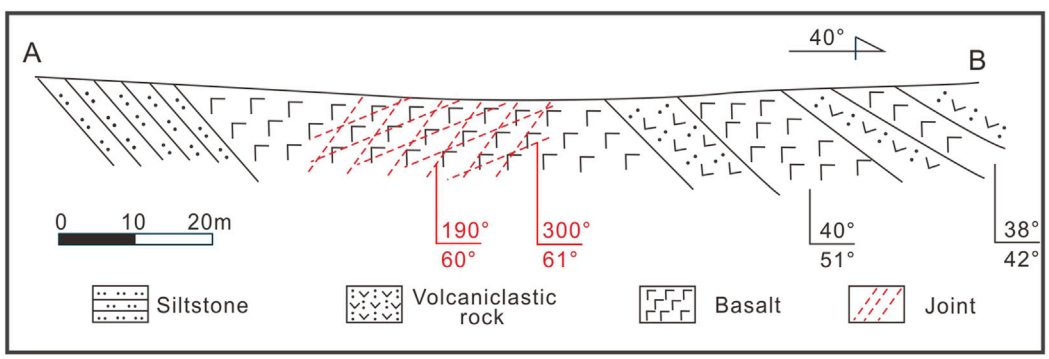

FIGURE 4 | Geological section of Longlin basalt among the Linghao Formation.

Resources [China University of Geosciences (Wuhan)], using a GeoLas 2005 excimer ArF laser ablation system coupled with a Neptune Plus GeoLas 2005 multi-collector (MC)-ICP-MS (Thermo Fisher Scientific). Analytical conditions include 32 μm beam size, 6 Hz frequency with an energy density of ~7 J/cm^2, and helium as the carrier gas. The standards (91,500 and GJ-1 zircon) were analyzed once for every eight zircon samples. Detail procedures for data calibration and processing are as described in Ye et al. (2013).

TABLE 1 | Major element (wt%) and trace element (ppm) compositions for the Longlin basalt samples.

Sample	TD-1	TD-4	ZD-4	ZD-7
wt%				
SiO_2	53.61	51.05	44.96	45.87
Al_2O_3	11.96	12.53	13.89	13.88
MgO	4.42	5.25	5.94	5.74
Na_2O	2.09	1.90	3.32	3.50
K_2O	2.07	2.58	1.27	1.22
P_2O_5	0.38	0.40	0.68	0.69
TiO_2	3.33	3.65	3.72	3.75
CaO	5.16	4.70	7.09	7.39
TFe_2O_3	12.68	13.25	15.92	15.02
MnO	0.18	0.19	0.21	0.22
LOI	3.76	4.09	2.93	2.68
ppm				
Li	12.2	13.6	13.8	12.7
Be	1.79	2.07	1.07	1.14
Sc	24.7	26.8	24.6	25.8
Ti	19,980	21,900	22,320	22,500
V	353	371	452	434
Cr	360	430	30	30
Mn	1250	1280	1410	1480
Co	33.6	37.2	49.2	44.3
Ni	85.6	96.6	43.6	41.4
Cu	98.4	104.5	95.3	86.5
Zn	118	131	120	95
Ga	23.2	24.3	22.4	22.0
As	8.1	9.7	7.9	7.5
Rb	73.7	65.1	19.9	18.2
Sr	1635	1005	484	453
Y	32.2	35.6	31.5	32.4
Zr	310	322	195	203
Nb	41.7	43.2	30.5	30.9
Sn	2.5	2.7	1.6	1.7
Ba	565	607	598	503
La	46.9	49.1	35.4	35.6
Ce	101.5	101.0	81.5	81.3
Pr	13.00	13.70	10.90	10.95
Nd	52.0	56.0	46.0	46.7
Sm	10.40	11.15	9.67	9.65
Eu	2.89	3.10	3.19	3.36
Gd	8.42	9.30	8.31	8.25
Tb	1.20	1.30	1.16	1.20
Dy	6.69	7.06	6.47	6.47
Ho	1.23	1.30	1.20	1.25
Er	3.14	3.40	3.13	3.19
Tm	0.42	0.46	0.44	0.43
Yb	2.54	2.62	2.51	2.61
Lu	0.37	0.40	0.38	0.37
Hf	7.7	7.9	4.8	4.9
Ta	2.43	2.56	1.80	1.88
Pb	7.8	6.9	0.8	0.8
Th	6.39	6.54	3.55	3.66
U	1.15	1.19	0.90	0.89
ΣREE	250.7	259.89	210.26	211.33
LREE	226.69	234.05	186.66	187.56
HREE	24.01	25.84	23.6	23.77
LREE/HREE	9.441482716	9.057662539	7.909322034	7.890618427
La_N/Yb_N	13.24	13.44	10.12	9.78
δEu	0.944166881	0.930692943	1.087929039	1.151256993
δCe	1.01	0.95	1.02	1.01

ANALYSIS RESULTS

Whole-Rock Major and Trace Element Geochemistry

In this study, we analyzed four fresh Longlin basalt samples (two samples from Tongdeng and Zhoudong each) for their whole-rock geochemical compositions (**Table 1**).

The basaltic rocks from Tongdeng and Zhoudong have SiO_2 = 51.05–53.61 wt% and 44.96–45.87 wt% and Al_2O_3 = 11.96–12.53 wt% and 13.88–13.89 wt%, respectively. Basalts from Tongdeng have clearly higher SiO_2 but lower Al_2O_3 contents. The Tongdeng samples have similar Na_2O and K_2O contents, i.e., Na_2O = 1.90–2.09 wt%, K_2O = 2.07–2.58 wt%, and Na_2O/K_2O = 0.74–1.01, whilst the Zhoudong samples have relatively high Na_2O and low K_2O, i.e., Na_2O = 3.32–3.50 wt%, K_2O = 1.22–1.27 wt%, and Na_2O/K_2O = 2.61–2.89. The Tongdeng samples have lower Fe [total iron (TFe_2O_3) = 12.68–13.25 wt%] and Mg (MgO = 4.42–5.25 wt%, Mg# = 41.08–44.21) than the Zhoudong samples (TFe_2O_3 = 15.02–15.92 wt%, MgO = 5.74–5.94 wt%, Mg# = 42.73–43.32). The Tongdeng and Zhoudong samples have TiO_2 = 3.33–3.65 wt% and 3.72–3.75 wt% and Ti/Y = 615–620 and 694–709, respectively, which fall into the high-Ti (Ti/Y) basalt (TiO_2 > 2.8%, Ti/Y > 500) range defined by Xu et al. (2001). In the Zr/TiO_2-Nb/Y and SiO_2-Nb/Y discrimination diagrams (**Figure 5**), all samples fall inside (near) the alkali basalt field.

The Tongdeng and Zhoudong samples have total REE (ΣREE) = 250.70–259.89 ppm and 210.26–211.33 ppm and La_N/Yb_N = 13.24–13.44 and 9.78–10.12, respectively. This indicates that the former has higher ΣREE and LREE/HREE fractionation than the latter. Samples from both Tongdeng and Zhoudong have indistinct Eu and Ce anomalies (**Figure 6A**; Tongdeng: δEu = 0.93–0.94, δCe = 0.95–1.01; Zhoudong: δEu = 1.09–1.15, δCe = 1.01–1.02). In the primitive mantle-normalized multi-element diagram (**Figure 6B**), the Zhoudong samples have distinct positive anomalies for some large ion lithophile elements (LILEs, e.g., Rb, K) and Sr, but negative anomalies in Nb and Y. In comparison, the Tongdeng samples have generally higher LILE contents, and have more distinct negative Sr and Zr-Hf contents than the Zhoudong samples. HREE contents of the Tongdeng and Zhoudong samples are similar.

The Longlin basalt samples have low loss on ignition (LOI = 2.68–4.09 wt%), indicating minimal alteration/weathering, which is consistent with the petrographic observation.

Zircon U-Pb-Hf Isotopes

Tongdeng Samples

Zircons (n = 28) from sample TD-1 show oscillatory zoning in cathodoluminescence (CL) images (**Figure 7A**). Most of them are 80–120 μm long and 60–90 μm wide with length: width ratio of 1.2–1.5. Results of the U-Pb isotopic dating are listed in **Table 2**. The zircons have Th/U = 0.43–0.87 (avg. 0.67). A total of 13 analysis spots clustered together along the U-Pb concordia (**Figure 7B**), yielding a weighted average age of 257.9 ± 2.6 Ma (MSWD = 0.55). 15 inherited zircons were also found, with ages of ca. 460–1811 Ma.

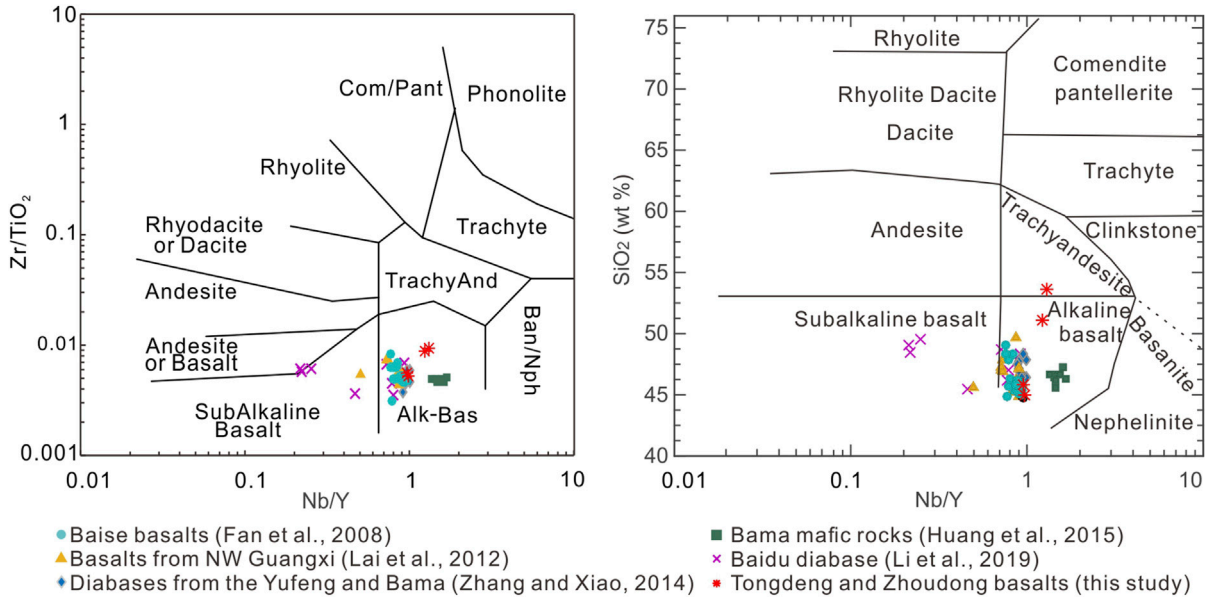

FIGURE 5 | (A) Zr/TiO_2-Nb/Y and **(B)** SiO_2-Nb/Y (Winchester and Floyd, 1977) discrimination diagrams for the mafic rocks from western Guangxi. Published data of other Late Permian mafic magmatic rocks in western Guangxi are also shown for comparison (Baise basalts, Fan et al., 2008; basalts from NW Guangxi, Lai et al., 2012; diabases from the Yufeng, and Bama, Zhang and Xiao, 2014; Bama mafic rocks, Huang et al., 2015; Baidu diabase, Li et al., 2019).

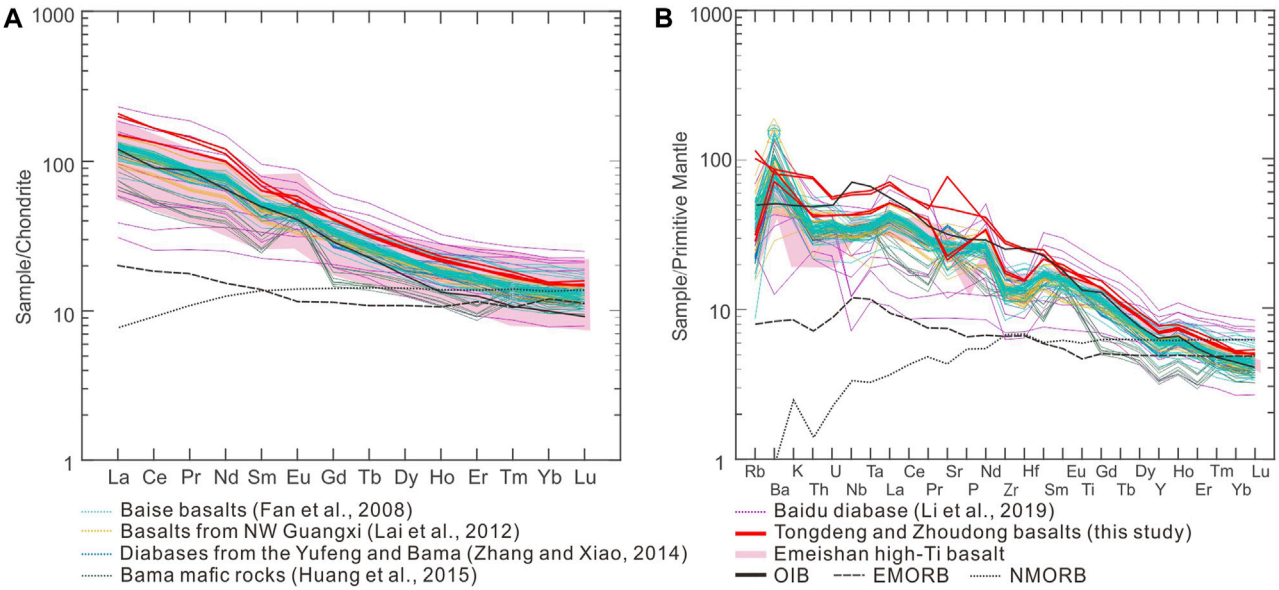

FIGURE 6 | (A) Chondrite-normalized REE and **(B)** primitive mantle normalized multi-element spidergram for the mafic rocks in western Guangxi (normalizing value after Sun and McDonough, 1989).

For the 29 Hf analysis spots (**Table 3**), 13 spots (with weighted average age of 257.9 Ma) yielded $^{176}Hf/^{177}Hf$ = 0.282245–0.282492. Calculated with their respective zircon U-Pb age, the zircons have εHf(t) = −13.22 to −4.15 (avg. −10.20) and one-stage model age (T_{DM1}) = 1,068–1,431 Ma (avg. 1,328 Ma). The remaining 15 analysis spots yielded $^{176}Hf/^{177}Hf$ = 0.281438–0.282658, and calculated εHf(t) = −14.44 to 11.48 and T_{DM} = 868–2,528 Ma.

Xiaoren Samples

Zircons (n = 30) from sample XR-1 show oscillatory zoning in CL images (**Figure 7C**). Most of them are 80–110 μm long and 50–80 μm with length: width ratio of 1.2–1.5. The zircons have high Th/U = 0.45–1.58 (avg. 0.76). All the data points fall on/near the concordia (**Figure 7D**), yielding a weighted average age of 259.6 ± 1.4 Ma (MSWD = 0.22) (**Table 2**). For Hf isotopes

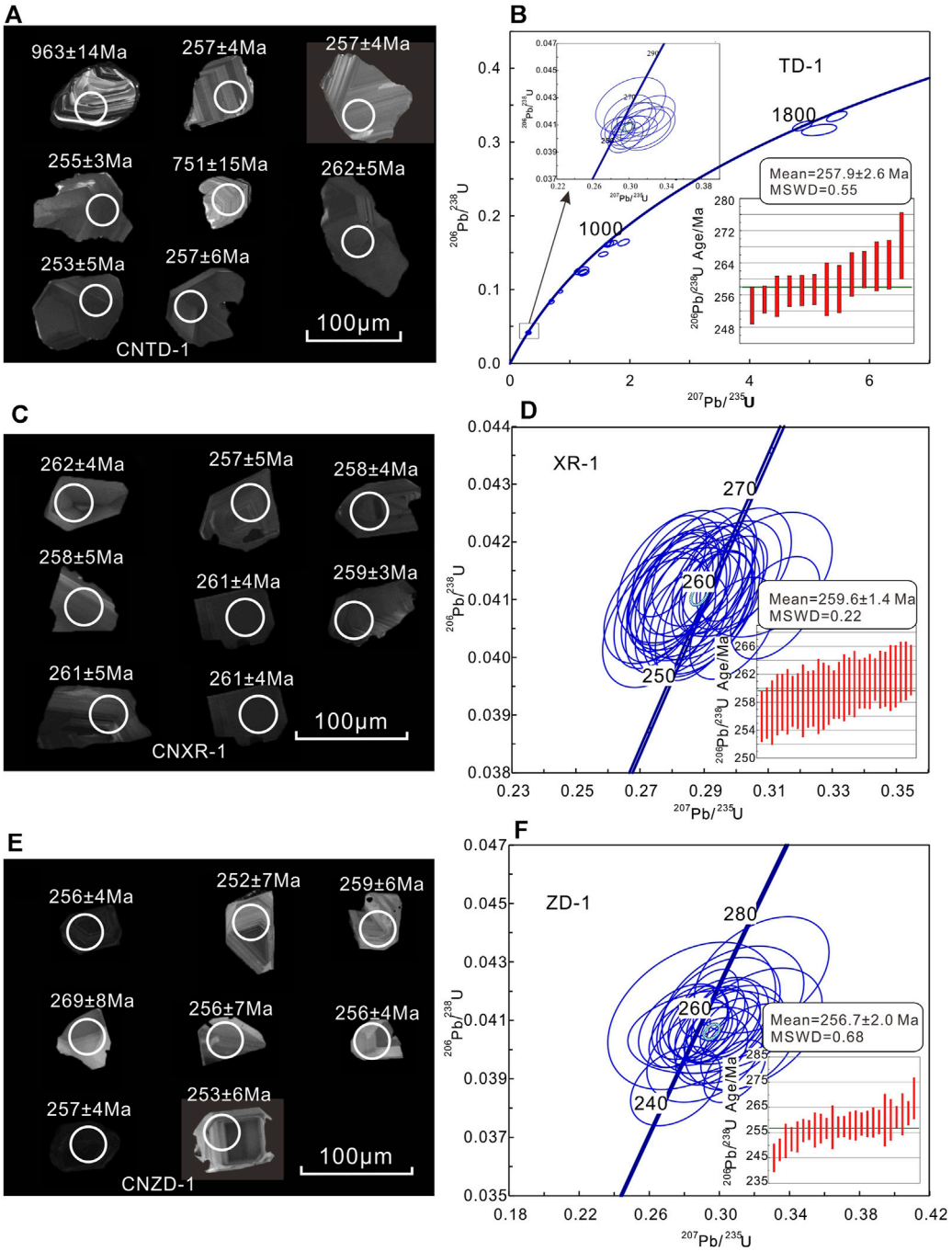

FIGURE 7 | Representative zircon CL image and concordia diagram for the Longlin basalt samples. The hollow ring is the position of analytical spot. Numbers near the analytical spots are the U-Pb ages (Ma).

(**Table 3**), 27 analysis spots yielded $^{176}Hf/^{177}Hf$ = 0.282353–0.282603, εHf(t) = −9.42 to −0.52 (avg. −4.83), and T_{DM1} = 924–1,294 Ma (avg. 1,109 Ma).

Zhoudong Samples

Zircons (*n* = 25) from sample ZD-1 show oscillatory zoning in CL images (**Figure 7E**). Most of them have length = 50–80 μm, width = 40–60 μm, and length: width ratio = 1.1–1.4, and have high Th/U = 0.32–1.87 (avg. 0.72). All the zircons cluster around the concordia and yielded a concordia age of 256.8 ± 1.1 Ma (MSWD = 9.5) (**Figure 7F**), which is similar to the weighted average age of 256.7 ± 2.0 Ma (MSWD = 0.68) (**Table 2**). For Hf isotopes (**Table 3**), 25 analysis spots yielded $^{176}Hf/^{177}Hf$ = 0.282607–0.282825, εHf(t) = −0.42 to 6.41 (avg. 3.10), and T_{DM} = 646–922 Ma (avg. 794 Ma).

TABLE 2 | Zircon La-ICP-MS U-Pb isotopic data for the Longlin basalt samples.

Analysis	Pb	Th	U	$^{207}Pb/^{206}Pb$		$^{207}Pb/^{235}U$		$^{206}Pb/^{238}U$		$^{207}Pb/^{206}Pb$		$^{207}Pb/^{235}U$		$^{206}Pb/^{238}U$	
		ppm		Ratio	1σ	Ratio	1σ	Ratio	1σ	Age (Ma)	1σ	Age (Ma)	1σ	Age (Ma)	1σ
TD-1-01	71	301	321	0.073983	0.001946	1.661195	0.045385	0.161161	0.002537	1043	54	994	17	963	14
TD-1-02	68	138	348	0.072091	0.001658	1.621626	0.039361	0.161001	0.002136	989	46	979	15	962	12
TD-1-03	75	57	193	0.108796	0.002333	4.881075	0.109199	0.321691	0.004352	1789	39	1799	19	1798	21
TD-1-04	17	242	312	0.054132	0.002959	0.306330	0.016354	0.040731	0.000607	376	119	271	13	257	4
TD-1-05	27	271	529	0.050400	0.002001	0.286202	0.011452	0.040664	0.000621	213	91	256	9	257	4
TD-1-06	18	157	362	0.051920	0.002165	0.289863	0.011063	0.040688	0.000616	283	96	258	9	257	4
TD-1-07	33	437	636	0.052019	0.001715	0.292051	0.009584	0.040330	0.000545	287	76	260	8	255	3
TD-1-08	151	153	366	0.116836	0.002303	5.456432	0.113420	0.334623	0.004545	1909	35	1894	18	1861	22
TD-1-09	62	160	310	0.072229	0.001739	1.630263	0.040341	0.161829	0.002242	992	49	982	16	967	12
TD-1-10	15	169	290	0.053942	0.002918	0.305018	0.016190	0.041339	0.000878	369	122	270	13	261	5
TD-1-11	23	142	129	0.071619	0.003122	1.214566	0.052878	0.123474	0.002527	976	89	807	24	751	15
TD-1-12	94	261	814	0.062729	0.001822	0.846737	0.023031	0.097000	0.001319	698	63	623	13	597	8
TD-1-14	38	29	403	0.058780	0.002296	0.686320	0.023430	0.084992	0.001419	567	85	531	14	526	8
TD-1-15	36	109	163	0.083518	0.003035	1.897084	0.063631	0.163738	0.002958	1281	71	1080	22	978	16
TD-1-16	57	189	287	0.075370	0.002619	1.556583	0.052045	0.147889	0.002129	1080	70	953	21	889	12
TD-1-17	34	522	620	0.052799	0.002367	0.300509	0.014478	0.040455	0.000814	320	102	267	11	256	5
TD-1-18	71	80	171	0.115803	0.004142	5.161256	0.192982	0.316251	0.005101	1892	64	1846	32	1771	25
TD-1-19	21	96	119	0.069590	0.004910	1.194028	0.080285	0.125381	0.003519	917	145	798	37	761	20
TD-1-21	24	317	435	0.055305	0.003643	0.314536	0.020712	0.040745	0.000959	433	116	278	16	257	6
TD-1-22	55	141	269	0.074524	0.002622	1.702454	0.057007	0.162877	0.002517	1057	71	1009	21	973	14
TD-1-23	25	266	465	0.056285	0.003486	0.322901	0.018443	0.041669	0.000990	465	137	284	14	263	6
TD-1-24	26	391	450	0.052257	0.003505	0.298829	0.017477	0.041732	0.000982	298	121	265	14	264	6
TD-1-25	28	153	156	0.071778	0.003146	1.235827	0.055249	0.122539	0.002656	989	90	817	25	745	15
TD-1-26	20	259	378	0.054136	0.003198	0.312633	0.017227	0.041529	0.000741	376	133	276	13	262	5
TD-1-27	38	523	707	0.053201	0.002552	0.296136	0.012746	0.040086	0.000746	345	105	263	10	253	5
TD-1-28	14	214	275	0.059202	0.004116	0.320732	0.019868	0.040741	0.001063	576	152	282	15	257	7
TD-1-29	24	90	247	0.059473	0.002428	0.693095	0.029176	0.082947	0.001634	583	89	535	17	514	10
TD-1-30	10	94	188	0.050696	0.004363	0.301635	0.025470	0.042495	0.001335	228	198	268	20	268	8
XR-1-01	19	266	382	0.053735	0.002350	0.309377	0.013623	0.041432	0.000713	361	100	274	11	262	4
XR-1-02	20	250	417	0.049315	0.002211	0.275965	0.011654	0.040597	0.000739	161	106	247	9	257	5
XR-1-03	23	333	443	0.048525	0.001907	0.274737	0.010551	0.040863	0.000640	124	93	246	8	258	4
XR-1-04	20	267	396	0.050880	0.002092	0.289243	0.011974	0.041000	0.000686	235	64	258	9	259	4
XR-1-05	19	258	384	0.050679	0.001821	0.282887	0.009481	0.040585	0.000587	233	81	253	8	256	4
XR-1-06	18	247	354	0.051519	0.001776	0.290333	0.010274	0.040868	0.000837	265	80	259	8	258	5
XR-1-07	20	216	421	0.049522	0.001750	0.282357	0.010448	0.041114	0.000651	172	83	253	8	260	4
XR-1-08	28	357	555	0.050115	0.001719	0.286213	0.009851	0.041316	0.000632	211	80	256	8	261	4
XR-1-09	23	211	487	0.051100	0.001834	0.289357	0.010863	0.040784	0.000707	256	83	258	9	258	4
XR-1-10	28	360	561	0.048900	0.001726	0.277317	0.010207	0.040976	0.000771	143	88	249	8	259	5
XR-1-11	22	275	426	0.049457	0.002235	0.282027	0.012568	0.041396	0.000757	169	106	252	10	261	5
XR-1-12	33	464	648	0.049237	0.001654	0.280739	0.009577	0.041205	0.000660	167	78	251	8	260	4
XR-1-13	23	345	428	0.051208	0.002266	0.289672	0.012517	0.040971	0.000866	250	102	258	10	259	5
XR-1-14	21	214	424	0.049939	0.001951	0.281216	0.010421	0.040850	0.000749	191	91	252	8	258	5
XR-1-15	15	192	308	0.050499	0.002024	0.285813	0.011441	0.041170	0.000770	217	93	255	9	260	5
XR-1-16	41	627	750	0.048329	0.001327	0.279146	0.007588	0.041579	0.000580	122	67	250	6	263	4
XR-1-17	19	183	401	0.049147	0.001658	0.281058	0.010025	0.041256	0.000761	154	80	251	8	261	5
XR-1-18	21	302	409	0.051535	0.001844	0.297106	0.011280	0.041362	0.000661	265	79	264	9	261	4
XR-1-19	12	174	235	0.052164	0.001926	0.300110	0.011310	0.041534	0.000695	300	85	266	9	262	4
XR-1-20	19	410	319	0.050710	0.001961	0.290096	0.010778	0.041561	0.000675	228	61	259	8	263	4
XR-1-21	29	372	568	0.048996	0.001407	0.282051	0.008180	0.041279	0.000581	146	67	252	6	261	4
XR-1-22	26	344	499	0.051325	0.001518	0.292345	0.008267	0.041016	0.000551	254	67	260	6	259	3
XR-1-23	14	204	264	0.049144	0.001694	0.277700	0.008950	0.040903	0.000649	154	81	249	7	258	4
XR-1-24	10	179	188	0.049998	0.001977	0.284489	0.011525	0.040920	0.000645	195	91	254	9	259	4
XR-1-25	41	675	748	0.050857	0.001317	0.294030	0.007823	0.041371	0.000631	235	64	262	6	261	4
XR-1-26	31	460	577	0.051704	0.001299	0.298694	0.007306	0.041361	0.000487	272	57	265	6	261	3
XR-1-27	30	759	480	0.054523	0.001544	0.312213	0.009177	0.040856	0.000585	394	63	276	7	258	4
XR-1-28	33	553	605	0.052665	0.001565	0.298959	0.008869	0.040506	0.000583	322	67	266	7	256	4
XR-1-29	28	482	508	0.051108	0.001290	0.294232	0.007173	0.041259	0.000563	256	57	262	6	261	3
XR-1-30	18	293	328	0.050963	0.001644	0.291304	0.009180	0.040834	0.000652	239	81	260	7	258	4
ZD-1-01	39	306	841	0.055512	0.002205	0.308840	0.011585	0.039262	0.000704	432	89	273	9	248	4
ZD-1-03	12	330	336	0.052805	0.003233	0.195868	0.010996	0.027045	0.000542	320	139	182	9	172	3
ZD-1-05	9	178	176	0.057653	0.003270	0.316499	0.017894	0.040089	0.000973	517	124	279	14	253	6
ZD-1-06	10	128	190	0.049682	0.002468	0.283362	0.014378	0.040918	0.000829	189	119	253	11	259	5
ZD-1-11	12	188	216	0.053998	0.004759	0.307796	0.026723	0.041523	0.001331	372	200	272	21	262	8

(Continued on following page)

TABLE 2 | (*Continued*) Zircon La-ICP-MS U-Pb isotopic data for the Longlin basalt samples.

Analysis	Pb	Th	U	$^{207}Pb/^{206}Pb$		$^{207}Pb/^{235}U$		$^{206}Pb/^{238}U$		$^{207}Pb/^{206}Pb$		$^{207}Pb/^{235}U$		$^{206}Pb/^{238}U$	
		ppm		Ratio	1σ	Ratio	1σ	Ratio	1σ	Age (Ma)	1σ	Age (Ma)	1σ	Age (Ma)	1σ
ZD-1-13	13	302	326	0.052522	0.003997	0.207544	0.015651	0.028673	0.000622	309	174	191	13	182	4
ZD-1-15	42	283	884	0.052178	0.001908	0.295049	0.010140	0.040521	0.000619	300	83	263	8	256	4
ZD-1-19	13	269	222	0.053908	0.004238	0.291651	0.021760	0.039828	0.001074	369	206	260	17	252	7
ZD-1-20	38	259	798	0.053033	0.002719	0.295749	0.013604	0.039940	0.000758	332	117	263	11	252	5
ZD-1-21	3	35	57	0.051343	0.005034	0.284236	0.031571	0.041154	0.001662	257	232	254	25	260	10
ZD-1-24	42	356	850	0.052432	0.002128	0.303630	0.012298	0.041348	0.000694	306	93	269	10	261	4
ZD-1-25	5	57	96	0.056262	0.004866	0.299513	0.023212	0.041173	0.001312	461	193	266	18	260	8
ZD-1-26	5	67	105	0.059686	0.004954	0.319396	0.025931	0.040699	0.001380	591	148	281	20	257	9
ZD-1-27	94	1628	3725	0.050122	0.001399	0.148207	0.004696	0.021115	0.000463	211	32	140	4	135	3
ZD-1-28	29	207	618	0.050826	0.002029	0.288251	0.011320	0.040712	0.000669	232	62	257	9	257	4
ZD-1-29	29	202	619	0.051312	0.001894	0.291135	0.010793	0.040626	0.000655	254	88	259	8	257	4
ZD-1-30	32	237	693	0.052272	0.001958	0.297918	0.011026	0.041031	0.000765	298	90	265	9	259	5
ZD-1-31	43	305	915	0.050757	0.001911	0.294113	0.011006	0.041594	0.000762	232	92	262	9	263	5
ZD-1-32	7	88	137	0.050652	0.003302	0.279244	0.016742	0.040815	0.000944	233	145	250	13	258	6
ZD-1-33	30	198	640	0.054044	0.002119	0.306291	0.011324	0.040748	0.000669	372	87	271	9	257	4
ZD-1-36	7	105	123	0.054228	0.003759	0.299376	0.018899	0.041010	0.000961	389	156	266	15	259	6
ZD-1-38	23	543	369	0.051093	0.004462	0.294296	0.030690	0.040618	0.000942	256	202	262	24	257	6
ZD-1-39	6	67	102	0.060346	0.006044	0.324208	0.025367	0.042553	0.001315	617	218	285	19	269	8
ZD-1-43	17	271	299	0.056477	0.004235	0.305951	0.020844	0.040526	0.001103	472	167	271	16	256	7
ZD-1-44	41	310	849	0.049012	0.002037	0.277313	0.011534	0.040490	0.000725	150	94	249	9	256	4
ZD-1-45	28	459	536	0.051000	0.003011	0.274991	0.016935	0.038751	0.000893	239	137	247	13	245	6
ZD-1-46	43	269	913	0.052999	0.002148	0.303627	0.012999	0.040909	0.000732	328	91	269	10	258	5
ZD-1-47	28	193	593	0.052049	0.003234	0.291269	0.016678	0.040798	0.000881	287	147	260	13	258	5

Note: σ is mean square error.

Whole-Rock Sr-Nd Isotopes

The Tongdeng samples have higher $(^{87}Sr/^{86}Sr)_i$ (0.707167–0.707345) but lower εNd(t) (−2.5 to −2.14) than the Zhoudong samples $(^{87}Sr/^{86}Sr)_i$ = 0.706181–0.706191, εNd(t) = 0.57–0.69 (**Table 4**). The Nd model age for the Tongdeng and Zhoudong samples are 1,227–1,217 Ma and 1,002–1,017 Ma, respectively. In the $(^{87}Sr/^{86}Sr)_i$-εNd(t) discrimination diagram (**Figure 8A**), all the Tongdeng and Zhoudong samples fall close to the MORB field and overlap with the Emeishan high-Ti basalts. In the εNd(t)-εHf(t) discrimination diagram (**Figure 8B**), the Tongdeng samples all fall far below the mantle evolution line, whilst the Zhoudong samples fall on or slightly below it.

DISCUSSION

Permian Mafic Magmatism in Western Guangxi

In this study, our new zircon LA-ICP-MS U–Pb dating results on three Longlin basalt samples yielded weighed mean $^{206}Pb/^{238}U$ age of 257.9 ± 2.6 Ma (Tongdeng), 259.6 ± 1.4 Ma (Xiaoren) and 256.7 ± 2.0 Ma (Zhoudong). Zircons in Longlin basalt are generally characterized by (weak) oscillatory zoning on CL images and high Th/U ratios (0.32–1.87), resembling typical magmatic zircons (Hoskin and Schaltegger, 2003). The Late Permian ages are consistent with the emplacement of these basalts among the Upper Permian Tonglinghao Formation. Therefore, the weighted mean $^{206}Pb/^{238}U$ ages of ca. 257–260 Ma can represent the crystallization age of the Longlin basalts. The older zircons (ca. 460–1811 Ma) in Longlin basalt are likely xenocrystic captured from the intruded wallrocks.

In recent years, many Late Permian magmatic rocks have been discovered in Western Guangxi. Fan et al. (2004) zircon SHRIMP U-Pb dated a basalt sample from Yangxu area and yielded a weighted mean $^{206}Pb/^{238}U$ age of 253.7 ± 6.1 Ma (n = 23, MSWD = 2.8). Fan et al. (2008) reported two zircon SHRIMP U-Pb ages of 259.5 ± 5.2 Ma (n = 14, MSWD = 5.0) and 259.1 ± 4.0 Ma (n = 7, MSWD = 0.85) from two basalts in the Bama area and Baise area. Lai et al. (2012) reported the zircon LA-ICP-MS U-Pb ages of 257 ± 9 Ma (n = 8, MSWD = 2.8) of another basalt sample from Bama area. Recently, Zhang and Xiao (2014) LA-ICP-MS zircon U-Pb dated two diabase sills from Yufeng and Bama and yielded weighted mean $^{206}Pb/^{238}U$ ages of 259.3 ± 0.8 Ma (n = 10, MSWD = 0.35) and $^{206}Pb/^{238}U$ ages of 257 6 ± 2.9 Ma (n = 12, MSWD = 1.06). Integrating these age data, mafic magmatism in the western Guangxi was probably active during ca. 254–260 Ma.

Petrogenesis of the Late Permian Western Guangxi Basalts

Crustal Assimilation

As shown in the $(^{87}Sr/^{86}Sr)_i$-εNd(t) diagram (**Figure 8A**), the samples plot above the evolutionary trend defined by mid-ocean ridge basalt (MORB) and lower or middle continental crust (LCC/MCC). This, and the relatively wide zircon εHf(t) range and linear correlations between MgO, Nb/La, and SiO_2 (**Figure 9**), suggest that parental magma may have experienced crustal assimilation during their ascent. Crustal

TABLE 3 | Zircon Hf isotopic data for the Longlin basalt samples.

Analysis	t (Ma)	$^{176}Yb/^{177}Hf$	$^{176}Lu/^{177}Hf$	$^{176}Hf/^{177}Hf$	1σ	εHf(t)	1σ	TDM1(Hf)	TDM2(Hf)
TD-1-20	240	0.112508	0.003099	0.282322	0.000013	−11.14	0.46	1390	1970
TD-1-27	253	0.097859	0.002856	0.282288	0.00001	−12.05	0.37	1431	2037
TD-1-7	255	0.0853	0.002464	0.282382	0.000013	−8.63	0.45	1279	1823
TD-1-17	256	0.099026	0.002945	0.282439	0.00001	−6.67	0.34	1212	1700
TD-1-5	257	0.110081	0.003339	0.282408	0.000012	−7.79	0.43	1271	1772
TD-1-6	257	0.028456	0.000836	0.282287	0.000009	−11.64	0.33	1356	2016
TD-1-4	257	0.041196	0.001317	0.282285	0.000012	−11.79	0.41	1376	2025
TD-1-28	257	0.03752	0.001152	0.282313	0.00001	−10.79	0.36	1331	1962
TD-1-21	257	0.04143	0.001253	0.282245	0.000011	−13.22	0.39	1430	2115
TD-1-10	261	0.033878	0.001038	0.282254	0.00001	−12.78	0.34	1410	2090
TD-1-26	262	0.035612	0.001093	0.282247	0.000011	−13.01	0.38	1421	2105
TD-1-23	263	0.077877	0.00232	0.282428	0.00001	−6.78	0.34	1206	1713
TD-1-24	264	0.054585	0.001762	0.28227	0.000012	−12.29	0.42	1414	2061
TD-1-30	268	0.021727	0.000756	0.282492	0.000009	−4.15	0.32	1068	1552
TD-1-29	514	0.025869	0.00082	0.282559	0.000008	3.5	0.3	976	1254
TD-1-14	526	0.023621	0.000773	0.282559	0.000009	3.78	0.31	975	1246
TD-1-12	597	0.025355	0.000812	0.282449	0.000016	1.41	0.55	1129	1450
TD-1-25	745	0.050102	0.001767	0.282444	0.00001	4	0.36	1165	1401
TD-1-11	751	0.062281	0.002132	0.282658	0.00001	11.48	0.36	868	932
TD-1-19	761	0.016123	0.000672	0.282002	0.000008	−10.76	0.29	1743	2339
TD-1-16	889	0.037597	0.00114	0.282229	0.000008	−0.22	0.28	1448	1776
TD-1-2	962	0.028373	0.000938	0.282002	0.000012	−6.56	0.44	1755	2228
TD-1-1	963	0.027836	0.001054	0.282308	0.000011	4.24	0.38	1334	1553
TD-1-9	967	0.027851	0.00092	0.282183	0.00001	−0.04	0.35	1504	1824
TD-1-22	973	0.037762	0.001278	0.28214	0.000012	−1.68	0.42	1579	1931
TD-1-15	978	0.015551	0.000544	0.281763	0.000009	−14.44	0.3	2063	2729
TD-1-18	1771	0.017903	0.000601	0.281589	0.000012	−3.09	0.43	2304	2629
TD-1-3	1798	0.038284	0.001358	0.281672	0.000009	−0.46	0.33	2234	2487
TD-1-8	1861	0.028131	0.000892	0.281438	0.000009	−6.83	0.31	2528	2927
XR-1-28	256	0.110715	0.003341	0.282582	0.000021	−1.65	0.75	1010	1383
XR-1-5	256	0.043959	0.001378	0.282432	0.000008	−6.64	0.3	1171	1699
XR-1-2	257	0.045846	0.001429	0.28245	0.00001	−6.01	0.36	1147	1660
XR-1-9	258	0.037287	0.001238	0.282603	0.000009	−0.52	0.31	924	1314
XR-1-30	258	0.052244	0.001626	0.282353	0.000013	−9.42	0.46	1290	1876
XR-1-14	258	0.037546	0.001161	0.282431	0.000009	−6.57	0.32	1165	1697
XR-1-27	258	0.098276	0.003125	0.282572	0.000014	−1.95	0.51	1020	1404
XR-1-3	258	0.076727	0.002297	0.282479	0.000015	−5.1	0.52	1133	1603
XR-1-23	258	0.036711	0.001097	0.282585	0.000012	−1.13	0.44	947	1353
XR-1-24	259	0.030127	0.000965	0.282586	0.000014	−1.08	0.51	942	1349
XR-1-10	259	0.057407	0.00176	0.282423	0.000009	−6.96	0.31	1195	1721
XR-1-4	259	0.051023	0.001579	0.282455	0.000009	−5.78	0.31	1144	1647
XR-1-22	259	0.034962	0.001068	0.282434	0.000012	−6.43	0.43	1158	1689
XR-1-7	260	0.036827	0.001125	0.282446	0.000009	−6.02	0.32	1143	1663
XR-1-15	260	0.038532	0.001242	0.282456	0.000015	−5.68	0.54	1133	1642
XR-1-12	260	0.071761	0.00223	0.282447	0.000012	−6.15	0.44	1176	1671
XR-1-17	261	0.026176	0.000803	0.282442	0.00001	−6.1	0.35	1139	1669
XR-1-29	261	0.083299	0.002381	0.282603	0.000019	−0.65	0.69	953	1323
XR-1-21	261	0.050621	0.001585	0.282473	0.000011	−5.13	0.4	1119	1607
XR-1-8	261	0.048946	0.001499	0.282447	0.000011	−6.02	0.38	1153	1664
XR-1-26	261	0.053506	0.001677	0.282426	0.000013	−6.79	0.45	1188	1712
XR-1-18	261	0.059755	0.001853	0.282562	0.000016	−2	0.57	999	1410
XR-1-25	261	0.080771	0.002498	0.282518	0.000015	−3.68	0.54	1081	1516
XR-1-11	261	0.052477	0.001568	0.282431	0.000009	−6.59	0.31	1178	1700
XR-1-1	262	0.087635	0.002665	0.282583	0.000017	−1.41	0.59	991	1373
XR-1-19	262	0.075995	0.002342	0.282368	0.000012	−8.94	0.42	1294	1848
XR-1-16	263	0.050863	0.001418	0.282447	0.00001	−5.97	0.37	1150	1662
ZD-1-27	135	0.088365	0.002933	0.282319	0.000012	−13.34	0.41	1388	2029
ZD-1-3	172	0.033256	0.001155	0.282295	0.000011	−13.22	0.37	1356	2051
ZD-1-13	182	0.028187	0.001043	0.282347	0.00001	−11.15	0.34	1279	1928
ZD-1-45	245	0.168095	0.004771	0.282825	0.000018	6.51	0.64	672	857
ZD-1-1	248	0.05117	0.001892	0.282633	0.000014	0.22	0.49	898	1259
ZD-1-19	252	0.076251	0.002307	0.282769	0.000018	5.04	0.65	709	955
ZD-1-20	252	0.041787	0.001572	0.282699	0.000027	2.7	0.95	796	1105
ZD-1-5	253	0.06476	0.001964	0.282741	0.000012	4.13	0.44	744	1015

(Continued on following page)

TABLE 3 | (*Continued*) Zircon Hf isotopic data for the Longlin basalt samples.

Analysis	t (Ma)	$^{176}Yb/^{177}Hf$	$^{176}Lu/^{177}Hf$	$^{176}Hf/^{177}Hf$	1σ	εHf(t)	1σ	TDM1(Hf)	TDM2(Hf)
ZD-1-44	256	0.027206	0.00095	0.282639	0.000009	0.77	0.33	866	1230
ZD-1-15	256	0.033752	0.001184	0.28268	0.000009	2.17	0.33	814	1141
ZD-1-43	256	0.101104	0.00298	0.282737	0.000017	3.88	0.61	770	1033
ZD-1-38	257	0.073786	0.002218	0.282734	0.000019	3.93	0.66	758	1030
ZD-1-29	257	0.03739	0.001253	0.282647	0.000011	1.02	0.38	862	1215
ZD-1-26	257	0.033116	0.000993	0.282772	0.000011	5.48	0.38	680	932
ZD-1-28	257	0.038275	0.001372	0.282607	0.000015	–0.42	0.54	922	1307
ZD-1-33	257	0.027671	0.000933	0.282647	0.00001	1.07	0.34	855	1212
ZD-1-47	258	0.042357	0.001492	0.282625	0.00002	0.22	0.69	899	1267
ZD-1-32	258	0.042764	0.001193	0.282757	0.000011	4.93	0.39	705	967
ZD-1-46	258	0.026803	0.000902	0.282634	0.00001	0.65	0.35	872	1240
ZD-1-6	259	0.033849	0.000981	0.28274	0.00001	4.39	0.35	725	1002
ZD-1-36	259	0.037992	0.001101	0.282727	0.000011	3.93	0.38	745	1032
ZD-1-30	259	0.029077	0.000992	0.282659	0.00001	1.53	0.35	840	1184
ZD-1-21	260	0.036689	0.001033	0.282797	0.00001	6.41	0.36	646	874
ZD-1-25	260	0.066052	0.001866	0.282742	0.000012	4.32	0.43	740	1008
ZD-1-24	261	0.048586	0.001851	0.282695	0.000018	2.69	0.64	808	1112
ZD-1-11	262	0.079678	0.002417	0.28272	0.000013	3.5	0.47	783	1062
ZD-1-31	263	0.038586	0.001392	0.282674	0.000012	2.08	0.42	827	1152
ZD-1-39	269	0.045788	0.001428	0.282789	0.000012	6.25	0.42	664	892

Note: For the calculation of εHf(t) values, we have adopted the ^{176}Lu decay constant of 1.867 × 10^{-11} (Söderlund et al., 2004), the present-day chondritic values of $^{176}Lu/^{177}Hf$ = 0.0332 and $^{176}Hf/^{177}Hf$ = 0.282772 (Blichert-Toft and Albarède, 1997). To calculate one-stage model ages (T_{DM1}) relative to a depleted-mantle source, we have adopted the present-day depleted-mantle values of $^{176}Lu/^{177}Hf$ = 0.0384 and $^{176}Hf/^{177}Hf$ = 0.28325 (Vervoort and Blichert-Toft, 1999).

TABLE 4 | Whole-rock Sr and Nd isotopic compositions for the Longlin basalt samples.

Sample	TD-1	TD-3	ZD-1	ZD-2-4
Sr (ppm)	1048	741	959	499
Rb (ppm)	67.9	75.1	64.9	20.5
$^{87}Rb/^{86}Sr$	0.09648	0.2486	0.1603	0.1604
$^{87}Sr/^{86}Sr$	0.7077	0.70808	0.70678	0.70677
2σ	0.00002	0.00002	0.00002	0.00001
$(^{87}Sr/^{86}Sr)_i$	0.7071709	0.7070046	0.706065	0.7063355
Nd (ppm)	66.0	60.6	46.4	47.4
Sm (ppm)	11.72	11.40	10.03	9.96
$^{147}Sm/^{144}Nd$	0.1174	0.1194	0.1223	0.1217
$^{143}Nd/^{144}Nd$	0.512376	0.512398	0.512542	0.512547
2σ	0.000003	0.000003	0.000003	0.000005
$(^{143}Nd/^{144}Nd)_i$	0.512178	0.512196	0.512335	0.512341
$\varepsilon_{Nd}(t)$	–2.167846	–1.949417	0.2974821	0.5097659
T_{DM} (Ma)	1110.948	1148.448	1116.7554	1063.0548
T_{2DM} (Ma)	1205.9407	1188.1823	1004.4052	987.12358

Note: $(^{87}Sr/^{86}Sr)_i$ and $(^{143}Nd/^{144}Nd)_i$ are the initial isotopic ratios of $^{87}Sr/^{86}Sr$ and $^{143}Nd/^{144}Nd$.

assimilation would have increased the Th/Ta ratios (cf. MORB and OIB: Th/Ta < 1.6, Sun and McDonough, 1989), as found in both the Tongdeng (Th/Ta = 2.55–2.63) and Zhoudong (Th/Ta = 1.95–1.97) samples. The Tongdeng samples may have had stronger crustal assimilation influence as their Th/Ta ratios are clearly higher than their Zhoudong counterparts. This conclusion is also supported by the higher SiO_2 and Nb/La, the lower MgO, zircon εHf(t) and whole-rock εNd(t) values, together with the more xenocrystic zircons in the Tongdeng samples.

If the rock formation was influenced by crustal assimilation, the rocks would have $(Th/Ta)_{PM} \approx 1$ and $(La/Nb)_{PM} > 1$ (by lower crustal material); and $(Th/Ta)_{PM} > 2$ and $(La/Nb)_{PM} > 2$ (by upper crustal material) (Peng et al., 1994). The Longlin basalts have $(Th/Ta)_{PM}$ = 0.94–1.27 and $(La/Nb)_{PM}$ = 1.17–1.20, showing mainly lower crustal influence. In the ($^{87}Sr/^{86}Sr)_i$-εNd(t) discrimination diagram (**Figure 8A**), the Longlin basalts plot above the evolutionary trend defined by MORB and LCC/MCC, indicating also lower crustal involvement. Assuming that the Longlin basalts were depleted mantle-derived, zircon Hf isotope calculation indicates that crustal input is of 8% for the Zhoudong samples and 40% for the Tongdeng samples. In the magma mixing modelling, the εHf(t) value of the depleted mantle-derived, ancient crustal-derived, and parental magmas of the Longlin basalts are 16 [depleted mantle εHf(t) value at 259 Ma], −13.22 [minimum measured Longlin basalt εHf(t) value] and −1/−10 [average measured Zhoudong/Tongdeng basalt εHf(t) value], respectively. The assumed Hf contents of the depleted mantle and crustal material are 0.309 μg/g (Taylor et al., 1981) and 4.5 μg/g (Yangtze middle-lower crustal average; Chi and Yan, 2007), respectively. Considering that the mantle-sourced parental magma of the Longlin basalts has lower/equal εHf(t) value than/to that of the depleted mantle, and that the assimilated crustal material has lower εHf(t) value than the lowest εHf(t) value (−13.22) of the samples, the Zhoudong and Tongdeng samples should have their actual degree of crustal assimilation below 8 and 40%, respectively.

The Lu-Hf and Sm-Nd isotopic systems have similar geochemical characteristics, and hence the εHf(t) and εNd(t) values show strongly positive correlation (Vervoort et al., 1999). Nd-Hf decoupling of magmatic rocks are commonly related to residual garnet or zircon enrichment in the magma source region (Patchett et al., 2004; Vervoort et al., 2000; Zeng et al., 2021a), and/or crustal assimilation (Patchett et al., 1984; Carpentier et al., 2009). From **Figure 8B**, it is shown that the Tongdeng samples

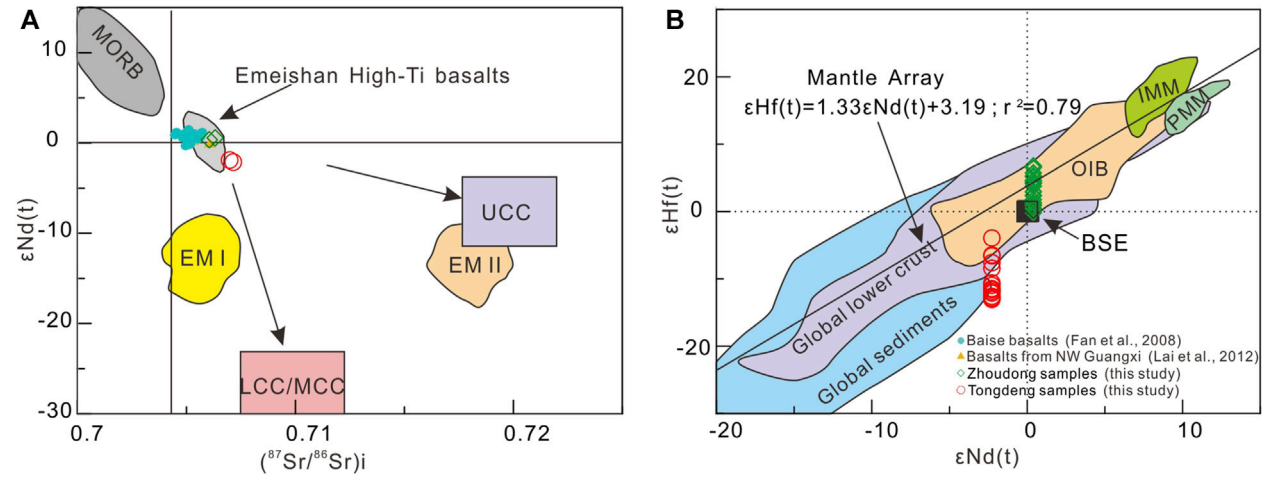

FIGURE 8 | (A) ($^{87}Sr/^{86}Sr)_i$-εNd(t) and **(B)** εHf(t)-εNd(t) (base map after Vervoort et al., 1999 and Zeng et al., 2021a; Zeng et al., 2021b) diagrams for the Longlin basalt samples. MORB, mid-ocean-ridge basalt; EM I and EM II, enriched mantle; HIMU, LCC/MCC, middle to lower continental crust; UC, upper continental crust; IMM, Indian MORB; PMM, Pacific MORB. Data source: the ranges of Emeishan high- and low-Ti basalts are from Xu et al. (2001), Zhou et al. (2006) and Xiao et al. (2003), Xiao et al. (2004)a,b; DM, EM I, and EM II (Zindler and Hart, 2003); LCC, MCC, and UC (Jahn et al., 1999); global sediments from Vervoort et al. (1999); global lower crust from Vervoort et al. (2000); IMM and PMM from Kempton et al. (2012).

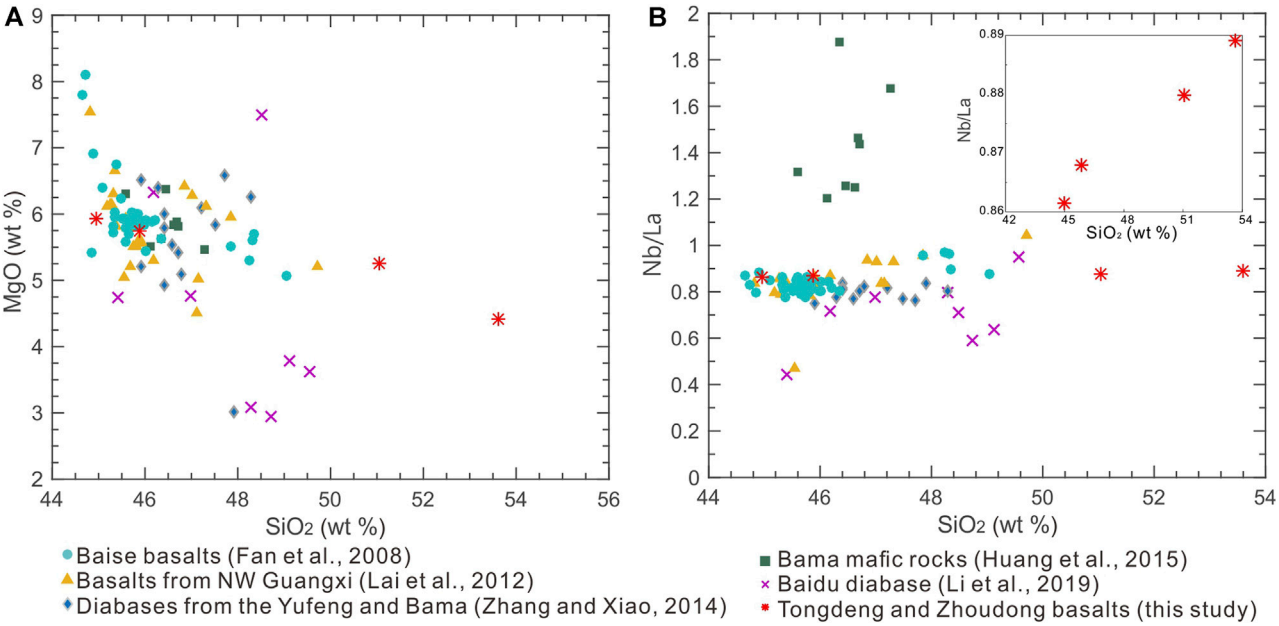

FIGURE 9 | (A) SiO_2-MgO and **(B)** Nb/La-SiO_2 diagrams for the Longlin basalt samples.

have clear Nd-Hf decoupling, whereas for the Zhoudong samples such decoupling is indistinct. Because not all samples of the Longlin basalts show Nd-Hf decoupling, the decoupling is probably unrelated to the mantle source region. As aforementioned, the Zhoudong samples have higher degree of crustal assimilation than the Tongdeng samples, implying that their Hf-Nd isotope decoupling was likely assimilation related. Since Hf^{4+} and Zr^{4+} have similar ionic radii, Hf is commonly enriched in zircon through isomorphism, leading to very low zircon Lu/Hf value (distinct lower than most rock-forming minerals) (Vervoort et al., 2011). After prolonged accumulation, εHf(t) of zircon would be clearly lower than that of other minerals, and thus the sediments or rocks with high zircon contents would have lower εHf(t) than those that lack zircon (e.g., mudstone, shale, or pelagic sediments) (Patchett et al., 1984; Carpentier et al., 2009). Meanwhile, the Sm-Nd

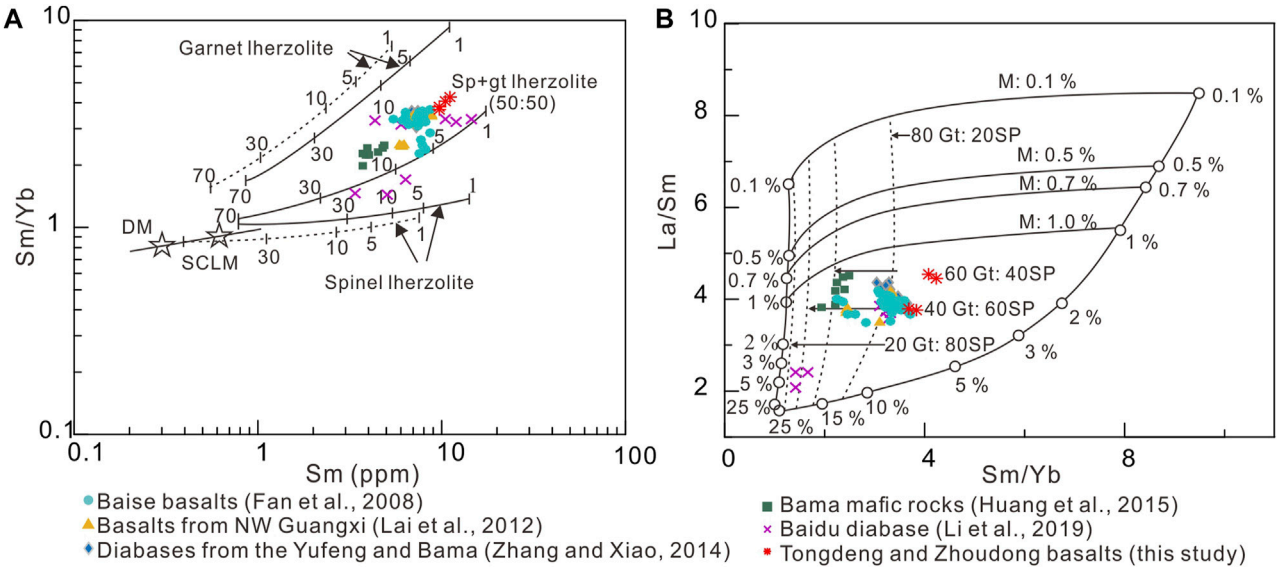

FIGURE 10 | (A) Sm/Yb-Sm diagram (dashed and solid lines are the melting trends for depleted mantle and enriched subcontinental lithospheric mantle, respectively. The numbers beside the lines are degrees of partial melting for a given mantle source); **(B)** La/Sm-Sm/Yb discrimination diagram for the Longlin basalt samples (After Özdemir and Güleç, 2014; M:0.7, M:1, M:2, M:3, and M:5% represents mixing lines between 0.7, 1, 2, 3 and 5% melts of garnet and spinel peridotite. Dashed lines indicate the relative proportions of melts derived from garnet and spinel peridotite mantle sources contributing to the parental magmas). Data from other basalt units in western Guangxi are shown for comparison.

isotope system is unaffected by zircon. Hence, the εHf(t) value of zircon-rich sediments or rocks would deviate negatively from its εNd(t) value with reference to the mantle array, whereas the εHf(t) value of zircon-poor sediments or rocks would deviate positively from its εNd(t) value with reference to the mantle array. The εHf(t) values of the Tongdeng sample are obviously lower than its εNd(t) value, indicating that the crustal materials assimilated by it should be zircon-rich sediments or rocks. The lesser crustal assimilation for the Zhoudong samples may have caused the indistinct Hf-Nd decoupling.

The content of REE in the crust is higher than that in the mantle (Taylor and McLennan, 1985; Sun and McDonough, 1989). Therefore, compared with the Zhoudong samples, the Tongdeng samples experienced stronger crustal contamination, which may be one of the reasons for their higher REE content. In addition, the contents of Zr and Hf in Tongdeng samples are obviously higher than Zhoudong samples, which is consistent with the fact that the crustal materials assimilated by them are rich in zircon.

Fractional Crystallization

It is generally considered that mantle-sourced primitive melts may have had relatively high Ni (> 400 ppm), Cr (> 1,000 ppm) and Mg# (73–81) contents (Mahoney, 1997; Wilson, 1989), which are not found in the Longlin basalts (Tongdeng: Ni = 12–22 ppm, Cr = 20–110 ppm, Mg# = 54–69; Zhoudong: Ni = 111–129 ppm, Cr = 220–280 ppm, Mg# = 58–60). This shows that fractionation of mafic minerals (e.g., olivine and pyroxene) has likely occurred (Frey and Prinz, 1978; Wang et al., 2016; Zeng et al., 2021b). Due to the insufficient element geochemical data, it is hard to determine the fractionated minerals from the Harker-type diagrams. Using the lowest Cr content of mantle-sourced melt (1,000 ppm; Wilson, 1989), calculation suggests that the petrogenesis of the Tongdeng samples requires ~50% olivine or ~20% pyroxene fractionation, whilst that of the Zhoudong samples requires ~30% olivine or ~10% pyroxene fractionation (partition coefficient from GERM website: http://www.earthref.org/). Because crustal assimilation can also reduce the magma Cr content, the degree of crystallization differentiation of mafic minerals in Zhoudong and Tongdeng samples must be lower than the above calculated values, especially the Tongdeng samples with higher degree of crustal contamination. The lack of Eu anomalies in the Longlin basalts indicates insignificant plagioclase fractionation.

Nature of Magma Source

All Longlin basalt samples in this study have lower εHf(t) and εNd(t) values than the depleted mantle, suggesting that the basaltic magma has undergone crustal assimilation during the magma ascent, and/or the magma was sourced from the mantle metasomatized by subducting crustal material, possibly from the altered Paleotethyan slab (Zeng et al., 2018; Xu et al., 2021).

The magma source region can be determined by the most primitive samples of the Longlin basalts (i.e., Zhoudong samples, with the least crustal assimilation and fractionation). Since Yb is more compatible in garnet than in pyroxene and spinel, whilst Sm is incompatible in all these minerals, Sm/Yb can also be used to constrain the mantle source mineralogy (Aldanmaz et al., 2000). In the Sm vs. Sm/Yb diagram (**Figure 10A**), the Zhoudong samples plot between the partial melting curves of garnet lherzolite and spinel-garnet facies (1:1) lherzolite. From the Sm/Yb vs. La/Sm diagram (**Figure 10B**) (Özdemir and Güleç, 2014), the

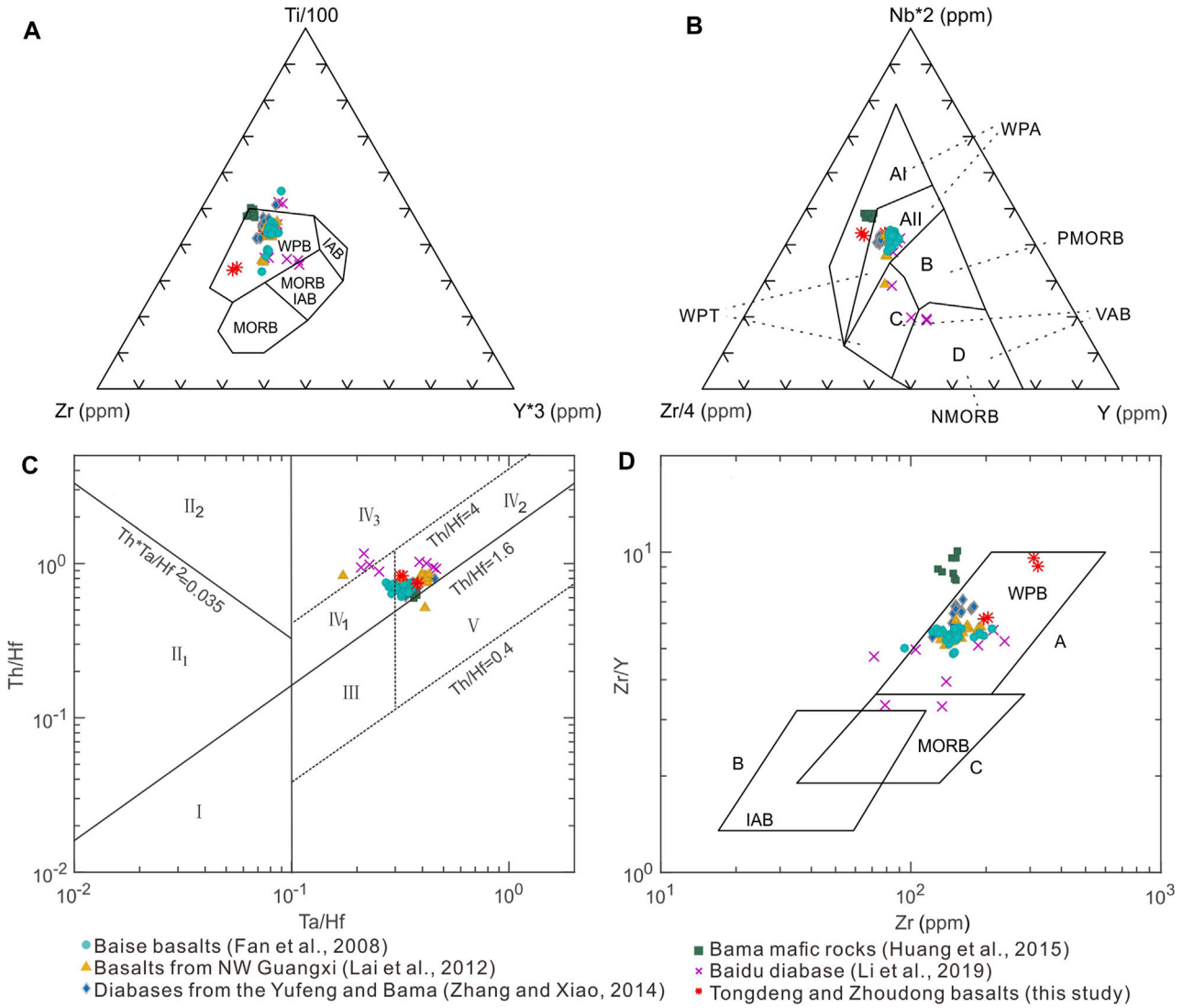

FIGURE 11 | Tectonic discrimination diagrams for the Longlin basalt samples: **(A)** Ti/100-Zr-Y*3 diagram (after Pearce and Cann, 1973); **(B)** Nb*2-Zr/4-Y diagram (after Meschede, 1986); Th/Hf-Ta/Hf diagram (after Wang et al., 2001); Zr/Y-Zr diagram (after Pearce, 1982). Data from other basalt units in western Guangxi are shown for comparison. WPB–within-plate basalt; MORB–mid-ocean ridge basalt; IAB–island-arc basalt; WPA–within-plate alkali basalts; WPT–within-plate tholeiites; VAB–volcanic-arc basalts; PMORB–basalt from plume-influenced regions; NMORB–oceanic basalt from normal mid-ocean ridge environment. **(C)**: I—N-MORB Margin of divergent oceanic plate; II—Margin of convergent plate (II_1—Island are of continental margin; II_2—Volcanic are of continental margin); III—Oceanic intra plate (the oceanic island and seamount, T-MORB, E-MORB); IV—Continental intraplate (IV_1—Continental rift; IV_2— Alkaline basalt zone; IV_3—Tensional zone); V—Mantle plume; **(D)** 1—Continental rift; 2—Continental tensional zone.

compositions of Longlin basalt are consistent with magmas formed by low-degree melting (1.0–2.0%) and >80% garnet lherzolite contribution. It is commonly accepted that the depth of the garnet-spinel stability zone is 75–85 km in the upper mantle (McKenzie and O'Nions, 1991; Klemme and O'Neill, 2000). Therefore, magma for Longlin basalt was likely formed in the spinel–garnet transition zone at 75–85 km depths.

Geodynamic Significance

In many tectonic discrimination diagrams (**Figure 11**), the Longlin basalts fall inside the within-plate basalt field, similar to most mafic rocks from western Guangxi. According to Sun et al. (2007), within-plate basalts have w (Nb)/w (Zr) > 0.04 and w (Th)/w (Nb) > 0.11, of which continental rift-related basalts and continental extension-related basalts have w (Th)/w (Nb) = 0.11–0.27 and >0.27 (generally 0.27–0.67), respectively. The Longlin basalts have their Nb/Zr (0.13–0.16) similar to that of within-plate basalts and their w (Th)/w (Nb) (0.12–0.15) similar to that of continental rift-related basalts of the within-plate basalts. This shows that the Late Permian western Guangxi was located in a continental rifting setting.

Based on ^{40}Ar-^{39}Ar dating, Hou et al. (2006) considered that the Emeishan LIP mafic magmatism occurred at ~258.9 Ma and

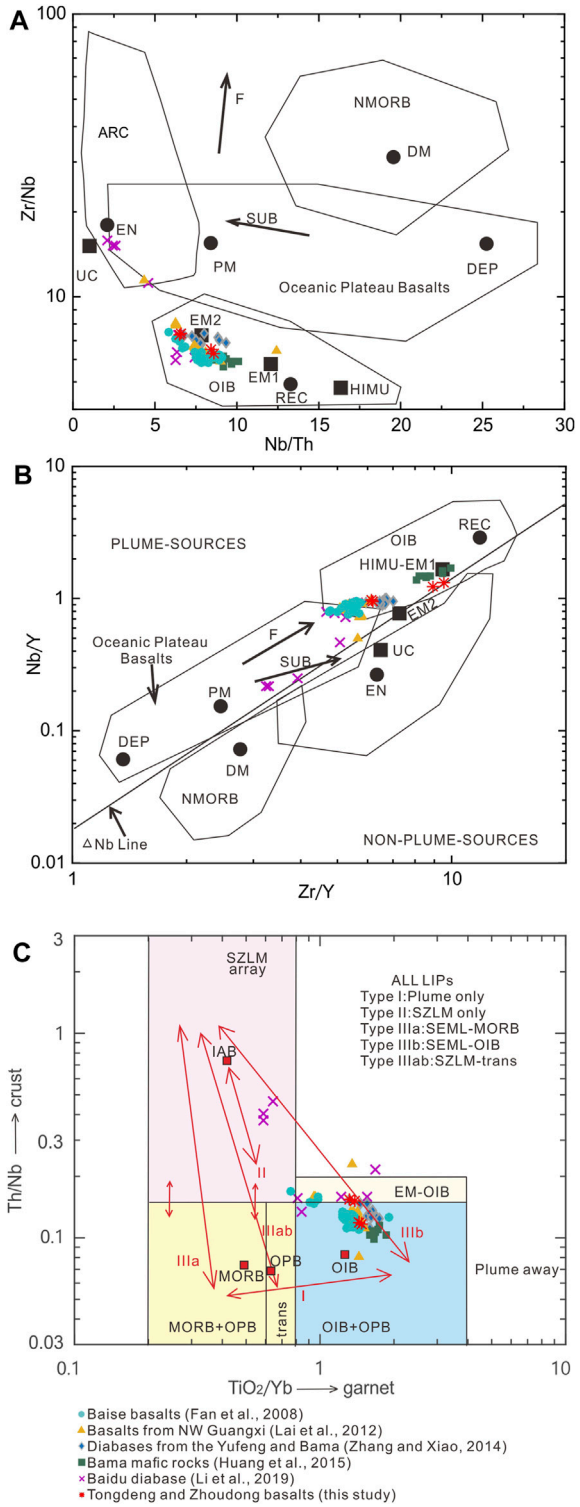

FIGURE 12 | (A) Nb/Th-Zr/Nb diagram (after Condie, 2005); **(B)** Zr/Y-Nb/Y diagram (after Condie, 2005); **(C)** TiO2/Yb-Th/Nb diagram (after Pearce et al., 2021). UC–upper continental crust; PM–primitive mantle; DM–shallow depleted mantle; HIMU–high mu (U/Pb) source; EM1 and EM2—enriched mantle sources; ARC–arc related basalts; NMORB–normal ocean ridge basalt; OIB–oceanic island basalt; DEP–deep depleted mantle; EN–enriched component; REC–recycled component; OPB–oceanic plateau basalt; IAB–island arc basalt.

lasted for less than 3 My. Shellnutt et al. (2008) constrained the timing of the Emeishan LIP plume activity to ~260 Ma. He et al. (2007) dated Xuanwei Formation, silicic ignimbrite and tuff by SHRIMP zircon geochronology, and considered that the activity time of Emeishan basalt is 259–262 Ma. Li (2012) statistically analyzed 70 age data of the Emeishan LIP magmatism, and found that the age was mostly concentrated in 252–265 Ma. As mentioned above, the Late Permian mafic magmatism was also developed in the western Guangxi, and its emplacement age was coeval with the Emeishan LIP magmatism. Moreover, the interpreted intraplate rift setting for the Late Permian mafic magmatism in western Guangxi is consistent with the rift setting of the Emeishan LIP. Previous studies indicate that the intermediate and outer zones of the Emeishan LIP comprise mainly high-Ti basalts (Xu et al., 2004; Cheng et al., 2019). The mafic magmatic rocks in western Guangxi generally have the high Ti-feature (Fan et al., 2008; Lai et al., 2012; Zhang and Xiao, 2014; Huang et al., 2015) and have similar Sr-Nd isotopic composition to the Emeishan high-Ti basalts (**Figure 8A**), which is consistent with its location in the Emeishan LIP margin. Hence, the Late Permian magmatism in western Guangxi is most likely associated with the Emeishan LIP.

Considering the role of mantle plume and lithosphere in the CFB formation, Turner et al. (1996) divided the CFB into two genetic types, i.e., Deccan-type and Parana-type. Deccan-type CFB has geochemical characteristics similar to OIB, which is derived from decompression melting of asthenospheric peridotite in the mantle plume. The Parana-type CFB is rich in incompatible elements, and is formed by partial melting of the lithospheric mantle (driven by mantle plume-derived heating). As shown in **Figure 6**, the Late Permian basalts in western Guangxi are enriched in LILEs and LREEs, with no discernible Nb, Ta and Ti anomalies. The distribution curves are obviously different from NMORB and EMORB, but similar to OIB. In addition, the Late Permian basalt samples in western Guangxi fall mainly in the OIB field (**Figure 12**). Therefore, we suggest that the Late Permian basalt in western Guangxi belongs to the Deccan-type, and its formation is closely related to the decompression melting of a mantle plume. In the Th/Nb-TiO_2/Yb diagram (**Figure 12C**), most of the western Guangxi basalt samples fall near the type-IIIB line (plume-SZLM interactions), which also demonstrates a mantle plume source with lithospheric input. This is consistent with our conclusion that the Longlin mafic magma has experienced crustal assimilation.

Possible formation mechanisms for the Emeishan high-Ti and low-Ti basalts are still under debate, and have been attributed to the different magma source regions, degrees of partial melting, fractional crystallization, and crustal assimilation processes, or a combination of these factors (e.g., Xu et al., 2001; Hao et al., 2004; Li et al., 2008; Zhang, 2009). In this study, formation of the Tongdeng and Zhoudong samples have clearly different degrees of crustal assimilation, yet they all have high-Ti features, which shows no obvious

relation between the high-Ti features and crustal assimilation. Since Fe-Ti oxides commonly fractionated at the late magma evolution stage (when MgO < 4 wt%) (Xu et al., 2013). The Zhoudong basalt samples have MgO > 4.42 wt%, which suggests that the high-Ti features are unlikely to be related to ilmenite fractionation. As afore-discussed, Late Permian basalts from western Guangxi (e.g., Longlin) were mainly sourced from low-degree partial melting of the mantle in the spinel–garnet transition zone, features that may have shaped their high-Ti characters. Since lithospheric thinning is commonly present above the mantle plume axis, partial melting could have extended to shallower depths (e.g., spinel stability field) and become more extensive (i.e., higher-degree partial melting). Conversely, distal from the mantle plume head, the lithospheric mantle is thicker and mantle decompression melting occurred at greater depths (in the spinel–garnet transition zone and garnet stability field) with lower intensity (i.e., low-degree partial melting). Therefore, the location of western Guanxi basalts on the Emeishan LIP margin may explain the high-Ti character of the basalts in this region.

High-Ti and low-Ti basalts also coexist in other LIPs around the world, such as the Paraná, Deccan, and Siberia (Peate et al., 1999; Xia et al., 2012). Fodor (1987) and Arndt et al. (1993) considered that high-Ti and low-Ti basalts are caused by different degrees of melting of the same mantle source, with the degree of partial melting degree for high-Ti basalts being lower than their low-Ti counterparts. McKenzie and Bickle (1988) suggested that the lithospheric mantle thickness is the principal factor that controls the depth and degree of partial melting in the mantle source region. Xia et al. (2012) considered that high-Ti basalts are formed by lower degree of partial melting in the deeper part of the mantle plume (tail), whereas low-Ti basalts are formed by higher degree of partial melting in the shallower part of the mantle plume (head). The above viewpoints are consistent with our conclusion that the difference of mantle source depth and degree of partial melting have caused the significant Ti content variation of magmatic rocks in the Emeishan LIP.

CONCLUSIONS

1) Longlin basalts from different places in western Guangxi yielded similar Late Permian zircon U-Pb ages, i.e., 257.9 ± 2.6 Ma (Tongdeng), 259.5 ± 0.75 Ma (Xiaoren), and 256.7 ± 2.0 Ma (Zhoudong), coeval with the Emeishan flood basalt emplacement.
2) Element and Sr-Nd-Hf isotope geochemistry show that the Longlin basalts were formed from low-degree partial melting in the spinel–garnet transition zone at depths of 75–85 km. The parental magma may have undergone mafic mineral (e.g., olivine and pyroxenes) fractionation and varying degrees of lower crustal assimilation.
3) Late Permian basalts in western Guangxi have similar emplacement age and geochemical features to the Emeishan high-Ti flood basalts. This suggests that the Emeishan LIP activity extended to western Guangxi.
4) Late Permian basalts in western Guangxi have OIB-type geochemical characteristics, and their formation is closely linked to the decompression melting of a mantle plume. The high-Ti features may have caused by the low-degree partial melting in the deep mantle.

DATA AVAILABILITY STATEMENT

The original contributions presented in the study are included in the article, further inquiries can be directed to the corresponding author.

AUTHOR CONTRIBUTIONS

CGZ and RYZ designed the research and drafted the manuscript. CML and JJ collected and processed the data. XJS prepared **Figures 1–12**. TGW contributed to the interpretation of the results.

FUNDING

This research was funded by the National Nature Science Foundation of China (41772349 and 42030809), Open Research Fund Program of State Key Laboratory of Nuclear Resources and Environment (East China University of Technology) (2020NRE13), the research grants from the East China University of Technology (DHBK2017103), Open Research Fund Program of Key Laboratory of Metallogenic Prediction of Nonferrous Metals and Geological Environment Monitoring (Central South University), Ministry of Education (2019YSJS08), the Key Scientific and Technological Research Project of Henan Province, China (192102310268), and the Nanhu Scholars Program for Young Scholars of XYNU.

ACKNOWLEDGMENTS

The authors would like to thank the Chief Editors Profs. David R. Lentz (Economic Geology) and Valerio Acocella (Volcanology), Guest Editor Dr. Chunkit Lai, and two reviewers for their insightful and constructive comments.

REFERENCES

Acocella, V. (2021). *Volcano-Tectonic Processes*. Switzerland: Springer, 1–552. doi:10.1007/978-3-030-65968-4

Aldanmaz, E., Pearce, J. A., Thirlwall, M. F., and Mitchell, J. G. (2000). Petrogenetic Evolution of Late Cenozoic, Post-Collision Volcanism in Western Anatolia, Turkey. *J. Volcanology Geothermal Res.* 102, 67–95. doi:10.1016/S0377-0273(00)00182-7

Andersen, T. (2002). Correction of Common Lead in U–Pb Analyses that Do Not Report 204Pb. *Chem. Geology.* 192 (1), 59–79. doi:10.1016/S0009-2541(02)00195-X

Arndt, N. T., Czamanske, G. K., Wooden, J. L., and Federenko, V. A. (1993). Mantle and Crustal Contributions to Continental Flood Volcanism. *Tectonophysics* 223, 39–52. doi:10.1016/0040-1951(93)90156-E

Blichert-Toft, J., and Albarède, F. (1997). The Lu-Hf Isotope Geochemistry of Chondrites and the Evolution of the Mantle-Crust System. *Earth Planet. Sci. Lett.* 148, 243–258. doi:10.1016/S0012-821X(97)00040-X

Carpentier, M., Chauvel, C., Maury, R. C., and Mattielli, N. (2009). The "Zircon Effect" as Recorded by the Chemical and Hf Isotopic Compositions of Lesser Antilles Forearc Sediments. *Earth Planet. Sci. Lett.* 287 (1-2), 86–99. doi:10.1016/j.epsl.2009.07.043

Cheng, W. B., Dong, S. Y., Jin, C. H., Zhao, B., Zhang, Y., and Wang, C. (2019). Characteristics of Elemental Geochemistry and Petrogenesis Discussion of the Emeishan Basalts in Muchuan Area, Sichuan Province. *J. Mineral. Petrol.* 39 (04), 49–60. (in Chinese). doi:10.19719/j.cnki.1001-6872.2019.04.06

Chi, Q. H., and Yan, M. C. (2007). *Handbook of Elemental Abundance for Applied Geochemistry*. Beijing: Geological Publishing House, 1–148. (in Chinese).

Chung, S.-L., and Jahn, B.-m. (1995). Plume-Lithosphere Interaction in Generation of the Emeishan Flood Basalts at the Permian-Triassic Boundary. *Geol.* 23 (10), 889. doi:10.1130/0091-7613(1995)023<0889:pliigo>2.3.co;2

Coffin, M. F., and Eldholm, O. (1994). Large Igneous Provinces: Crustal Structure, Dimensions, and External Consequences. *Rev. Geophys.* 32 (1), 1–36. doi:10.1029/93RG02508

Courtillot, V. E., and Renne, P. R. (2003). On the Ages of Flood basalt Events. *Comptes Rendus Geosci.* 335 (1), 113–140. doi:10.1016/S1631-0713(03)00006-3

Duggen, S., Hoernle, K., Van Den Bogaard, P., and Garbe-schönberg, D. (2005). Post-Collisional Transition From Subduction- to Intraplate-Type Magmatism in the Westernmost Mediterranean: Evidence for Continental-Edge Delamination of Subcontinental Lithosphere. *J. Petrol.* 46 (6), 1155–1201. doi:10.1093/petrology/egi013

Fan, W., Zhang, C., Wang, Y., Guo, F., and Peng, T. (2008). Geochronology and Geochemistry of Permian Basalts in Western Guangxi Province, Southwest China: Evidence for Plume-Lithosphere Interaction. *Lithos.* 102, 218–236. doi:10.1016/j.lithos.2007.09.019

Fan, W. M., Wang, Y. J., Peng, T. P., Miao, L. C., and Guo, F. (2004). The Ar-Ar and U-Pb Chronology of Late Paleozoic Basalts in Western Guangxi and Their Constraints on the Emeishan Basalt Province Eruption Age. *Chi. Sci. Bull.* 49 (18), 1892–1900. (in Chinese)

Fodor, R. V. (1987). Low- and High-TiO2 Flood Basalts of Southern Brazil: Origin From Picritic Parentage and a Common Mantle Source. *Earth Planet. Sci. Lett.* 84 (4), 423–430. doi:10.1016/0012-821X(87)90007-0

Frey, F. A., and Prinz, M. (1978). Ultramafic Inclusions From San Carlos, Arizona: Petrologic and Geochemical Data Bearing on Their Petrogenesis. *Earth Planet. Sci. Lett.* 38 (1), 129–176. doi:10.1016/0012-821X(78)90130-9

Goldstein, S. L., O'Nions, R. K., and Hamilton, P. J. (1984). A Sm-Nd Isotopic Study of Atmospheric Dusts and Particulates From Major River Systems. *Earth Planet. Sci. Lett.* 70, 221–236. doi:10.1016/0012-821X(84)90007-4

Halpin, J. A., Tran, H. T., Lai, C.-K., Meffre, S., Crawford, A. J., and Zaw, K. (2016). U-pb Zircon Geochronology and Geochemistry from NE Vietnam: A 'Tectonically Disputed' Territory Between the Indochina and South China Blocks. *Gondwana Res.* 34, 254–273. doi:10.1016/j.gr.2015.04.005

Hao, Y. L., Zhang, Z. C., Wang, F. S. M., and Mahoney, J. J. (2004). Petrogenesis of High-Ti and Low-Ti Basalts From the Emeishan Large Igneous Province. *Geol. Rev.* 50 (6), 587–592. (in Chinese). doi:10.16509/j.georeview.2004.06.005

He, B., Xu, Y.-G., Huang, X.-L., Luo, Z.-Y., Shi, Y.-R., Yang, Q.-J., et al. (2007). Age and Duration of the Emeishan Flood Volcanism, SW China: Geochemistry and SHRIMP Zircon U-Pb Dating of Silicic Ignimbrites, Post-Volcanic Xuanwei Formation and clay Tuff at the Chaotian Section. *Earth Planet. Sci. Lett.* 255 (3-4), 306–323. doi:10.1016/j.epsl.2006.12.021

He, B., Xu, Y. G., Chung, S. L., Long, X., and Wang, Y. (2003). Sedimentary Evidence for a Rapid, Kilometer-Scale Crustal Doming Prior to the Eruption of the Emeishan Flood Basalts. *Earth Planet. Sci. Lett.* 213 (3-4), 391–405. doi:10.1016/S0012-821X(03)00323-6

Hoskin, P. W. O., and Schaltegger, U. (2003). 2. The Composition of Zircon and Igneous and Metamorphic Petrogenesis. *Rev. mineralogy Geochem.* 53 (1), 27–62. doi:10.2113/053002710.1515/9781501509322-005

Hou, T., Zhang, Z. C., Kusky, T., Du, Y. S., Liu, J. L., and Zhao, Z. D. (2011). A reappraisal of the high-Ti and low-Ti classification of basalts and petrogenetic linkage between basalts and mafic-ultramafic intrusions in the Emeishan Large Igneous Province, SW China. *Ore Geol. Rev.* 41 (1), 133–143. doi:10.1016/j.oregeorev.2011.07.005

Hou, Z. Q., Chen, W., and Lu, J. R. (2006). The 259Ma Continental Overflow Basalt Eruption Event in Emeishan Large Diagenetic Province, Sichuan, China: Evidence From Laser 40Ar/39Ar Dating. *Acta Geologica Sinica.* 8, 1130, 2006. (in Chinese).

Huang, W. L., Liu, X. J., Shi, Y., Xu, J. F., Liao, S., Guo, L., et al. (2015). Geochemistry of Extreme High Ti/Y Mafic Rocks from Western Guangxi: Implications for the Primitive Magma of High Ti basalt of Emeishan Mantle Plume? *Geol. Bull. China.* 34 (2/3), 474–486. CNKI:SUN:ZQYD. (in Chinese).

Jacobsen, S. B., and Wasserburg, G. J. (1980). Sm-Nd Isotopic Evolution of Chondrites. *Earth Planet. Sci. Lett.* 50, 139–155. doi:10.1016/0012-821X(84)90109-2

Jahn, B. M., Wu, F. Y., Lo, C. H., and Tsai, C. H. (1999). Crust–Mantle Interaction Induced by Deep Subduction of the Continental Crust: Geochemical and Sr–Nd Isotopic Evidence From Post-Collisional Mafic–Ultramafic Intrusions of the Northern Dabie Complex, Central China. *Chem. Geology.* 157 (1–2), 119–146. doi:10.1016/S0009-2541(98)00197-1

Kempton, P. D., Pearce, J. A., Barry, T. L., Fitton, J. G., Langmuir, C., and Christie, D. M. (2002). Sr-Nd-Pb-Hf Isotope Results From ODP Leg 187: Evidence for Mantle Dynamics of the Australian-Antarctic Discordance and Origin of the Indian MORB Source. *Geochem.-Geophys.-Geosyst.* 3 (12), 1–35. doi:10.1029/2002GC000320

Klemme, S., and O'Neill, H. S. (2000). The Near-Solidus Transition From Garnet Lherzolite to Spinel Lherzolite. *Contrib. Mineral. Petrol.* 138 (3), 237–248. doi:10.1007/s004100050560

Lai, S., Qin, J., Li, Y., Li, S., and Santosh, M. (2012). Permian High Ti/Y Basalts From the Eastern Part of the Emeishan Large Igneous Province, Southwestern China: Petrogenesis and Tectonic Implications. *J. Asian Earth Sci.* 47, 216–230. doi:10.1016/j.jseaes.2011.07.010

Li, C. M., Qin, H. F., and Jiang, J. (2019). Regional Geological Survey Report of Longlin (Nanning, China). *Guangxi Geol. Surv. Inst.* 1–336. (in Chinese).

Li, H. B. (2012). Mantle Plume Geodynamic Significances of the Emeishan Large Igneous Province: Evidence from Mafic Dykes, Geochemistry and Stratigraphic Records. *China Univ. Geosciences.*, 1–185. (in Chinese).

Li, J., Xu, J. F., He, B., Xu, Y. G., and Dong, Y. H. (2008). Sr-Nd-Os Isotopic Geochemistry of Permian Picrites From Muliarea, Southeast Tibet. *Acta Petrologica Sinica.* 24 (02), 337–347. CNKI:SUN:YSXB. (in Chinese).

Liao, S., Liu, X. J., Shi, Y., Huang, W. L., and Guo, L. (2013). The Product of Interaction Between Mantle Plume and Island Arc Magma: Evidence From Basic Rocks in Diabase Gold Deposits in Western Guangxi. *Acta Minera Sinica.* 33 (S2), 111–113. (in Chinese). doi:10.16461/j.cnki.1000-4734.2013.s2.493

Liew, T. C., and Hofmann, A. W. (1988). Precambrian Crustal Components, Plutonic Associations, Plate Environment of the Hercynian Fold Belt of Central Europe: Indications From a Nd and Sr Isotopic Study. *Contrib. Mineral. Petrol.* 98, 129–138. doi:10.1007/BF00402106

Long, X., Yigang, X., Jifeng, X., Bin, H., and Franco, P. (2004). Chemostratigraphy of Flood Basalts in the Garzê-Litang Region and Zongza Block: Implications for Western Extension of the Emeishan Large Igneous Province, SW China. *Acta Geologica Sinica - English Edition.* 78, 61–67. doi:10.1111/j.1755-6724.2004.tb00675.x

Ludwig, K. R. (2003). User's Manual for Isoplot /Ex rev.3.00: A Geochronological Toolkit for Microsoft Excel, *Berkeley Geochronology Center.* 4. 1–70.

Lugmair, G. W., and Marti, K. (1978). Lunar Initial 143Nd/144Nd: Differential Evolution of the Lunar Crust and Mantle. *Earth Planet. Sci. Lett.* 39, 349–357. doi:10.1016/0012-821X(78)90021-3

Mahoney, J. J., and Coffin, F. (1997). *Large Igneous Provinces: Continental, Oceanic, and Planetary Flood Volcanism*. Washington, DC: American Geophysical Union, 273–295.

Mckenzie, D., and Bickle, M. J. (1988). The Volume and Composition of Melt Generated by Extension of the Lithosphere. *J. Petrology.* 29, 625–679. doi:10.1093/petrology/29.3.625

McKenzie, D., and O'Nions, R. K. (1991). Partial Melt Distributions From Inversion of Rare Earth Element Concentrations. *J. Petrology.* 32 (5), 1021–1091. doi:10.1093/petrology/32.5.1021

Meschede, M. (1986). A Method of Discriminating Between Different Types of Mid-Ocean Ridge Basalts and Continental Tholeiites With the Nb-Zr-Y Diagram. *Chem. Geology.* 56 (3-4), 207–218. doi:10.1016/0009-2541(86)90004-5

Nebel, O., Scherer, E. E., and Mezger, K. (2011). Evaluation of the 87Rb Decay Constant by Age Comparison Against the U-Pb System. *Earth Planet. Sci. Lett.* 301, 1–8. doi:10.1016/j.epsl.2010.11.004

Nicholas, T. A., Gerald, K. C., Joseph, L. W., and Valeri, A. F. (1993). Mantle and Crustal Contributions to Continental Flood Volcanism. *Tectonophysics.* 223, 39–52. doi:10.1016/0040-1951(93)90156-E

Özdemir, Y., and Güleç, N. (2014). Geological and Geochemical Evolution of the Quaternary Süphan Stratovolcano, Eastern Anatolia, Turkey: Evidence for the Lithosphere-Asthenosphere Interaction in Post-Collisional Volcanism. *J. Petrol.* 55 (1), 37–62. doi:10.1093/petrology/egt060

Patchett, P. J., Vervoort, J. D., Söderlund, U., and Salters, V. J. M. (2004). Lu-Hf and Sm-Nd Isotopic Systematics in Chondrites and Their Constraints on the Lu-Hf Properties of the Earth. *Earth Planet. Sci. Lett.* 222 (1), 29–41. doi:10.1016/j.epsl.2004.02.030

Patchett, P. J., White, W. M., Feldmann, H., Kielinczuk, S., and Hofmann, A. W. (1984). Hafnium/Rare Earth Element Fractionation in the Sedimentary System and Crustal Recycling into the Earth's Mantle. *Earth Planet. Sci. Lett.* 69 (2), 365–378. doi:10.1016/0012-821X(84)90195-X

Pearce, J. A., and Cann, J. R. (1973). Tectonic Setting of Basic Volcanic Rocks Determined Using Trace Element Analyses. *Earth Planet. Sci. Lett.* 19 (2), 290–300. doi:10.1016/0012-821X(73)90129-5

Pearce, J. A., Ernst, R. E., Peate, D. W., and Rogers, C. (2021). LIP Printing: Use of Immobile Element Proxies to Characterize Large Igneous Provinces in the Geologic Record. *Lithos.* 392-393, 106068. doi:10.1016/j.lithos.2021.106068

Pearce, J. A. (1982). Trace Element Characteristics of Lavas From Destructive Plate Boundaries. *John Willey & Sons.* 8, 525–548.

Peate, D. W., Hawkesworth, C. J., Mantovani, M. M. S., Rogers, N. W., and Turner, S. P. (1999). Petrogenesis and Stratigraphy of the High-Ti/Y Urubici Magma Type in the Parana Flood Basalt Province and Implications for the Nature of 'Dupal'-type Mantle in the South Atlantic Region. *J. Petrology.* 40, 451–473. doi:10.1093/petroj/40.3.451

Peng, Z. X., Mahoney, J., Hooper, P., Harris, C., and Beane, J. (1994). A Role for Lower Continental Crust in Flood Basalt Genesis? Isotopic and Incompatible Element Study of the Lower Six Formations of the Western Deccan Traps. *Geochimica et Cosmochimica Acta.* 58 (1), 267–288. doi:10.1016/0016-7037(94)90464-2

Sderlund, U., Patchett, P. J., and Vervoort, J. D. (2004). The 176Lu Decay Constant Determined by Lu–Hf and U–Pb Isotope Systematics of Precambrian Mafic Intrusions. *Earth Planet. Sci. Lett.* 219, 311–324. doi:10.1016/S0012-821X(04)00012-3

Shellnutt, J. G. (2014). The Emeishan Large Igneous Province: A Synthesis. *Geosci. Front.* 5 (3), 369–394. doi:10.1016/j.gsf.2013.07.003

Shellnutt, J. G., Zhou, M.-F., Yan, D.-P., and Wang, Y. (2008). Longevity of the Permian Emeishan Mantle Plume (SW China): 1 Ma, 8 Ma or 18 Ma? *Geol. Mag.* 145 (3), 373–388. doi:10.1017/S0016756808004524

Söderlund, U., Patchett, P. J., Vervoort, J. D., and Isachsen, C. E. (2004). The 176 Lu Decay Constant Determined by Lu–Hf and U–Pb Isotope Systematics of Precambrian Mafic Intrusions. *Earth Planet. Sci. Lett.* 219 (3), 311–324. doi:10.1016/S0012-821X(04)00012-3

Sun, S.-s., and McDonough, W. F. (1989). Chemical and Isotopic Systematics of Oceanic Basalts: Implications for Mantle Composition and Processes. *Geol. Soc. Lond. Spec. Publications.*, 42, 313–345. doi:10.1144/GSL.SP.1989.042.01.19

Sun, S. Q., Zhang, C. J., and Zhao, S. J. (2007). Identification of the Tectonic Settings for Continental Intraplate by Trace Elements. *Geotectonica et Metallogenia.* 31 (01), 104–109. (in Chinese). doi:10.16539/j.ddgzyckx.2007.01.012

Taylor, S. R., and Mclennan, S. M. (1985). The Continental Crust: its Composition and Evolution. *J. Geology.* 94 (4), 57–72.

Taylor, S. R., McLennan, S. M., Armstrong, R. L., and Tarney, J. (1981). The Composition and Evolution of the Continental Crust: Rare Earth Element Evidence From Sedimentary Rocks and Discussion. *Philosophical Trans. R. Soc. B Biol. Sci.* 301 (1461), 398–399. doi:10.1109/WFCS.2015.7160546

Turner, S., Hawkesworth, C., Gallagher, K., Stewart, K., Peate, D., and Mantovani, M. (1996). Mantle Plumes, Flood Basalts, and Thermal Models for Melt Generation Beneath Continents: Assessment of a Conductive Heating Model and Application to the Paraná. *J. Geophys. Res.* 101 (B5), 11503–11518. doi:10.1029/96JB00430

Vervoort, J. D., and Blichert-Toft, J. (1999). Evolution of the Depleted Mantle: Hf Isotope Evidence From Juvenile Rocks Through Time. *Geochimica et Cosmochimica Acta.* 63, 533–556. doi:10.1016/S0016-7037(98)00274-9

Vervoort, J. D., Patchett, P. J., Albarede, F., Blicherttoft, J., Rudnick, R. L., and Downes, H. (2000). Hf-Nd Isotopic Evolution of the Lower Crust. *Earth Planet. Sci. Lett.* 181 (1), 115–129. doi:10.1016/S0012-821X(00)00170-9

Vervoort, J. D., Patchett, P. J., Blichert-Toft, J., and Albarède, F. (1999). Relationships Between Lu–Hf and Sm–Nd Isotopic Systems in the Global Sedimentary System. *Earth Planet. Sci. Lett.* 168 (1–2), 79–99. doi:10.1016/S0012-821X(99)00047-3

Vervoort, J. D., Plank, T., and Prytulak, J. (2011). The Hf-Nd Isotopic Composition of marine Sediments. *Geochimica et Cosmochimica Acta.* 75 (20), 5903–5926. doi:10.1016/j.gca.2011.07.046

Wang, D. Z., and Zhou, J. C. (2005). New Progress in Studying the Large Igneous Provinces. *Geol. J. China Universities.* 11 (1), 1–8. CNKI:SUN:GXDX. (in Chinese)

Wang, L., Jin, X. B., Wang, X. Y., Wu, X. K., Liu, C. F., and Duan, G. L. (2015). Forming Process of Lamprophyre From Luocheng, Northern Guangxi: Constraints from Geochemistry, Geochronology and Sr-Nd-Pb Isotopes. *Geol. Sci. Technology Inf.* 34 (01), 10–19. CNKI:SUN:DZKQ (in Chinese).

Wang, L., Wang, G., Lei, S., Wang, W., Qing, M., Jia, L., et al. (2016). Geochronology, Geochemistry and Sr-Nd-Pb-Hf Isotopes of the Paleoproterozoic Mafic Dykes From the Wulashan Area, North China Craton: Petrogenesis and Geodynamic Implications. *Precambrian Res.* 286, 306–324. doi:10.1016/j.precamres.2016.09.009

Wang, Y. L., Zhang, C. J., and Xiu, S. Z. (2001). Th/Hf-Ta/Hf Identification of Tectonic Setting of Basalts. *Acta Petrologica Sinica.* 17 (3), 413–421. CNKI:SUN:YSXB(in Chinese).

Wang, Y., and Xing, C. M. (2018). Compositions of Clinopyroxenes From the Ertan High-Ti basalt and Baima Layered Intrusion of the Emeishan Large Igneous Province: Implication for a Genetic Link of the High-Ti basalt and Layered Intrusion. *Bull. Mineralogy, Petrology Geochem.* 37 (06), 1019–1034. (in Chinese). doi:10.19658/j.issn.1007-2802.2018.37.113

Wilson, M. (1989). *Igneous Petrogenesis*. London: SpringerHarper Collins Academic, 466.

Wu, H. R., Kuang, G. D., and Wang, Z. C. (1997). Preliminary Study on the Late Paleozoic Tectonic Sedimentary Setting in Guangxi. *Scientia Geologica Sinica.* 32 (1), 11–18. CNKI:SUN:DZKX (in Chinese).

Wu, H. R., Kuang, G. D., and Wang, Z. C. (1993). Reinterpretation of Basic Igneous Rocks in Western Guangxi and its Tectonic Implications. *Scientia Geologica Sinica.* 32 (3), 288–289. CNKI:SUN:DZKX (in Chinese).

Xia, L. Q., Xu, X. Y., Li, X. M., Xia, Z. C., and Ma, Z. P. (2012). Comparison of Three Large Igneous Provinces (Emeishan, Siberia, Deccan) in Asia. *Northwest. Geol.* 45(02), 1–26. (in Chinese)

Xiao, L., Xu, Y.-G., Chung, S.-L., He, B., and Mei, H. (2003). Chemostratigraphic Correlation of Upper Permian Lavas From Yunnan Province, China: Extent of the Emeishan Large Igneous Province. *Int. Geology. Rev.* 45 (6), 753–766. doi:10.2747/0020-6814.45.8.753

Xiao, L., Xu, Y. G., Mei, H. J., Zheng, Y. F., He, B., and Pirajno, F. (2004). Distinct Mantle Sources of Low-Ti and High-Ti Basalts From the Western Emeishan Large Igneous Province, SW China: Implications for Plume-Lithosphere Interaction. *Earth Planet. Sci. Lett.* 228 (3-4), 525–546. doi:10.1016/j.epsl.2004.10.002

Xu, J., Xia, X.-P., Wang, Q., Spencer, C. J., He, B., Lai, C.-K., et al. (2021). Low-δ18O A-Type Granites in SW China: Evidence for the Interaction Between the Subducted Paleotethyan Slab and the Emeishan Mantle Plume. *GSA Bull.* doi:10.1130/B35929.1

Xu, J., Xia, X. P., Lai, C. K., Zhou, M., Ma, P., and Ma, P. F. (2019). First Identification of Late Permian Nb-Enriched Basalts in Ailaoshan Region (SW Yunnan, China): Contribution From Emeishan Plume to Subduction of Eastern Paleotethys. *Geophys. Res. Lett.* 46 (5), 2511–2523. doi:10.1029/2018GL081687

Xu, Y.-G., He, B., Chung, S.-L., Menzies, M. A., and Frey, F. A. (2004). Geologic, Geochemical, and Geophysical Consequences of Plume Involvement in the Emeishan Flood-Basalt Province. *Geol.* 32 (10), 917–920. doi:10.1130/G20602.1

Xu, Y., Chung, S. L., Jahn, B. M., and Wu, G. (2001). Petrologic and Geochemical Constraints on the Petrogenesis of Permian–Triassic Emeishan Flood Basalts in Southwestern China. *Lithos.* 58 (3-4), 145–168. doi:10.1016/S0024-4937(01)00055-X

Xu, Y. G., He, B., Luo, Z. Y., and Liu, H. Q. (2013). Study of Mantle Plumes and Large Igneous Provinces in China: an Overview and Perspectives. *Bull. Mineralogy, Petrology Geochem.* 32 (01), 25–39. CNKI:SUN:KYDH (in Chinese).

Ye, X. F., Zong, K. Q., Zhang, Z. M., He, Z. Y., Liu, Y. S., Hu, Z. C., et al. (2013). Geochemistry of Neoproterozoic Granite in Liuyuan Area of Southern Beishan Orogenic belt and its Geological Significance. *Geol. Bull. China.* 32 (Z1), 307–317. CNKI:SUN:ZQYD (in Chinese).

Zeng, R.-Y., Lai, J.-Q., Mao, X.-C., Yan, J., Zhang, C.-G., and Xiao, W.-Z. (2021a). Geochemistry and Zircon Ages of the Yushigou Diabase in the Longshoushan Area, Alxa Block: Implications for Crust-Mantle Interaction and Tectonic Evolution. *Geol. Mag.* 158 (4), 685–700. doi:10.1017/S0016756820000783

Zeng, R. Y., Lai, J. Q., Mao, X. C., Xiao, W. Z., Yan, J., Zhang, C. G., et al. (2021b). Petrogenesis and Tectonic Significance of the Early Devonian Lamprophyres and Diorites in the Alxa Block, NW China. *Geochemistry.* 81, 125685. doi:10.1016/j.chemer.2020.125685

Zeng, R. Y., Lai, J. Q., Mao, X. C., Li, B., Zhang, J. D., Bayless, R., et al. (2018). Paleoproterozoic Multiple Tectonothermal Events in the Longshoushan Area, Western North China Craton and Their Geological Implication: Evidence from Geochemistry, Zircon U-Pb Geochronology and Hf Isotopes. *Minerals.* 8 (9), 361. doi:10.3390/min8090361

Zhang, B., Guo, F., Zhang, X., Wu, Y., Wang, G., and Zhao, L. (2019). Early Cretaceous Subduction of Paleo-Pacific Ocean in the Coastal Region of SE China: Petrological and Geochemical Constraints from the Mafic Intrusions. *Lithos.* 334-335, 8–24. doi:10.1016/j.lithos.2019.03.010

Zhang, X. J., and Xiao, J. F. (2014). Zircon U-Pb Geochronology, Hf Isotope and Geochemistry Study of the Late Permian Diabase in the Northwest Guangxi Autonomous Region. *Bull. Mineralogy, Petrology Geochem.* 33 (02), 163–176. (in Chinese). doi:10.3969/j.issn.1007-2802.2014.02.003

Zhang, Z. C. (2009). A Discussion on Some Important Problems Concerning the Emeishan Large Igneous Province. *Geology. China.* 36 (3), 634–646. CNKI:SUN:DIZI (in Chinese).

Zhang, Z. C., Wang, F. S., Fan, W. M., Deng, H. L., Xu, Y. G., Xu, J. F., et al. (2001). A Discussion on Some Problems Concerning the Study of the Emeishan Basalts. *Acta Petrologica et Mineralogica.* 20 (3), 239–246. CNKI:SUN:YSKW (in Chinese).

Zhou, M.-F., Zhao, J.-H., Qi, L., Su, W., and Hu, R. (2006). Zircon U-Pb Geochronology and Elemental and Sr-Nd Isotope Geochemistry of Permian Mafic Rocks in the Funing Area, SW China. *Contrib. Mineral. Petrol.* 151 (1), 1–19. doi:10.1007/s00410-005-0030-y

Zindler, A., and Hart, S. (1986). Chemical Geodynamics. *Annu. Rev. Earth Planet. Sci.* 14 (1), 493–571. doi:10.1146/annurev.ea.14.050186.002425

Conflict of Interest: The authors declare that the research was conducted in the absence of any commercial or financial relationships that could be construed as a potential conflict of interest.

Publisher's Note: All claims expressed in this article are solely those of the authors and do not necessarily represent those of their affiliated organizations, or those of the publisher, the editors and the reviewers. Any product that may be evaluated in this article, or claim that may be made by its manufacturer, is not guaranteed or endorsed by the publisher.

Copyright © 2021 Zhang, Zeng, Li, Jiang, Wang and Shi. This is an open-access article distributed under the terms of the Creative Commons Attribution License (CC BY). The use, distribution or reproduction in other forums is permitted, provided the original author(s) and the copyright owner(s) are credited and that the original publication in this journal is cited, in accordance with accepted academic practice. No use, distribution or reproduction is permitted which does not comply with these terms.